DSPACE

https://dspace.org/

Gold mineralisation potential of the Kraaipan granite-greenstone terrane, southern Botswana

Mdze, Manelisi

2023
https://hdl.handle.net/10539/35684

Downloaded from a DSpace repository. https://dspace.org/

UNIVERSITY OF THE WITWATERSRAND, JOHANNESBURG

Gold mineralisation potential of the Kraaipan granite-greenstone terrane, southern Botswana

By

Manelisi Mdze

(Student number: 1790711)

A project report submitted to the Faculty of Science at the University of the Witwatersrand to fulfil the requirements for the degree of Master of Science.

Declaration

I declare that this project report, titled "Gold mineralisation potential of the Kraaipan granite-greenstone terrane, southern Botswana" is my own work. It is submitted to the University of the Witwatersrand for the fulfilment of the degree of Master of Science. It has not been submitted at any other institution for examination.



9th day of March in 2023

Abstract

The Kraaipan granite-greenstone terrane, which straddles the North West province of South Africa and the Southern district of Botswana, is comprised of four linear, north-south trending greenstone belts namely, Stella, Kraaipan, Madibe and Amalia. Banded iron formation (BIF)-hosted gold mineralisation is present within the Kraaipan Greenstone Belt (KGB) in South Africa at the currently producing Kalahari Goldridge mine, as well as other defunct mines and historical occurrences. There are no known gold deposits along the Botswana extension of the KGB where the belt has a strike length of over 40 km.

A review of historical data suggests that the KGB is largely unexplored in Botswana, with most of the belt covered by younger strata (Transvaal Supergroup and Kalahari Group). To evaluate the gold potential of the KGB in Botswana, field mapping and observations were integrated with historical geological and exploration datasets to produce an updated geological interpretation of the KGB.

A Kalahari sediment thickness map was constructed from historical borehole data, to differentiate between areas of thicker and thinner cover. Thicker cover complicates mineral exploration, in particular the interpretation of soil geochemistry results and mining. Satellite imagery was used effectively for geological and regolith mapping. High-resolution Bing imagery was particularly effective at accurately mapping rock fabric, folds, and faults in areas of outcrop and sub-crop. Landsat 8 data was used to identify reflectance signatures associated with various types of regolith from which provenance predictions can be used to understand the nature and source of soil geochemical anomalies.

Magnetic data is the most effective geophysical dataset for mapping the KGB lithologies, including the high-interest gold-bearing BIF, due to a distinct magnetic response relative to the encompassing granitic rocks. Ultra-high-resolution magnetic data collected over part of the study area was used to: better resolve the extension of the KGB into the study area; accurately delineate lithological contacts and structures and to identify high-interest exploration target areas.

Down-hole multi-element data was evaluated from four drill-holes which historically intersected elevated gold mineralisation. In all instances the gold mineralisation was associated with greater than 15 weight-percent iron, confirming gold affinity with strongly iron-oxidised

rocks. Silver, copper, nickel, arsenic, antimony, selenium and bismuth displayed excellent down-hole correlations with gold, therefore their usefulness as gold pathfinder elements in this geological setting should not be disregarded.

Acknowledgements

I wish to thank my employer Mineral Services Botswana for not only allowing me to conduct this study but also funding it. In addition, they allowed me to use company resources and some of their own data, without which this research project would not exist. Dr Asinne Tshibubudze and Conrad Ocker provided invaluable feedback which helped to improve the thought process and structuring of this research project.

TABLE OF CONTENTS

1 Introduction 1
1.1 Background 1
1.2 Aims and Objectives 2
1.3 Report/Thesis Organization 3
2 Regional Geology 4
2.1 Greenstone rocks 5
2.2 Granitoids (granites and gneisses) 6
2.3 Deformation 8
2.4 Kraaipan granite-greenstone gold mineralisation 9
2.4.1 Kalahari Goldridge Mine 9
2.4.2 Blue Dot Deposit 11
3 Methodology 14
3.1 Magnetic data acquisition and interpretation 14
3.2 Kalahari isopach map 15
3.3 Photogeology and Remote Sensing 15
3.4 Geological field mapping and ground-truthing 16
4 Historical data review 18
4.1 Geophysical survey data 18
4.2 Kalahari isopach mapping 22
4.3 Geological mapping 24
4.3.1 Satellite imagery and remote sensing 24
4.3.2 Field mapping 30
4.4 Geochemical data and analysis 34
4.4.1 Geochemistry from soil samples 35
4.4.2 Historical Drilling results 41
5 Discussion 48
5.1 BIF hosted gold deposits 48
5.1.1 Homestake Mine 48
5.1.2 Challenger Deposit 51
5.2 General geology and the potential for Kraaipan gold exploration 53
6 Conclusions 60
7 References 62

LIST OF FIGURES

Figure 1. Locality map showing the study area as well as the greenstone belts. 2

Figure 2. Distribution of the various greenstone belts and fragments on the Kaapvaal Craton. 5

Figure 3. Map depicting a generalised geological map of the Kraaipan granite-greenstone terrane within the Kimberly Block of the Kaapvaal Craton. 7

Figure 4. Overview map of the Kalgold Mine; a cross-section of the D-Zone deposit; and some drill intersections 10

Figure 5. Group II veins occurring within the mineralised and altered BIF 11

Figure 7. Maps depicting different filter images of regional magnetic data collected at 250 m line-spacing or wider. 19

Figure 8. Maps of the area with supposed north-western extension of the Kaaipan Greenstone Belt where high-resolution magnetic data was collected. 22

Figure 9. Location maps of historical boreholes from which Kalahari thicknesses were derived. 23

Figure 10. Maps depicting interpolated Kalahari isopach maps. 24

Figure 11. High-resolution Bing satellite imagery over an area of rock exposure, and the structures mappable from the image 25

Figure 12. Landsat-8 colour composite images, where the linear north-south BIF outcrop occurs within the yellow outline. 27

Figure 13. Spectral reflectance of jarosite, hematite and geothite (from the USGS Spectral Library). 28

Figure 14. Thematic map generated through supervised classification from Landsat 8 band1-7 multispectral data, using ground-truthed RIOs. 29

Figure 15. Different rocks units that were encountered during field mapping. 31

Figure 16. Photographs displaying some of the structural features that were observed during field mapping. 33

Figure 17. Geological maps of the southern part of the study area, created from field mapping and satellite imagery. 34

Figure 18. Locations of historical soil samples with assay results within the study area. 36

Figure 19. Soil sample results for the ‘Soil sampling 1’ programme are overlain on a Bing satellite image 38

Figure 20. Location maps of ‘Soil sampling 2’ programme soil samples overlain on an SRTM image. 41

Figure 21. Locations of historical boreholes within the Kraaipan Greenstone Belt. 43

Figure 22. Down-hole geochemical logs of four boreholes containing historical gold intersections. 47

Figure 23. Maps depicting an overview of the Homestake Mine locality as well as the geology of the mine area and ore deposit. 50

Figure 25. A: vertical profiles of Au and Ca in calcrete samples within the Challenger deposit. 53
Figure 26. Interpretation maps of the NW area of the Kraaipan Greenstone Belt where high-resolution magnetic data was collected. 56
Figure 27. Distribution patterns of selected elements in regolith along a section overlying the D-Zone orebody of Kalgold mine. 58

LIST OF TABLES

Table 1. Correlation matrix of Au, Cu and Ni for the “Soil sampling 1” programme. 37

Table 2. "Soil sampling 2" correlation matrix for selected potential gold pathfinder elements. 39

Table 3. Summary of Reunion Mining’s historical gold mineralisation intersections within the Kraaipan greenstone belt of Botswana. 42

Table 4. Summary of Laconia Resources' mineral intercepts within the Kraaipan Greenstone Belt of Botswana. 43

LIST OF ABBREVIATIONS AND ACRONYMS

AS	Analytical Signal
BIF	Banded Iron Formation
ECW	Enhanced Compression Wavelet
Esri	Environmental Systems Research Institute
FVD	First Vertical Derivative
GFAAS	Graphite Furnace Atomic Absorption Spectrometry
GPS	Global Positioning System
JPEG	Joint Photographic Experts Group
Kalgold	Kalahari Goldridge
KGB	Kraaipan Greenstone Belt
MLEM	Moving Loop Electromagnetics
PNG	Portable Network Graphics
ppb	parts per billion
ppm	parts per million
QGIS	Quantum Geographic Information System
ROI	Region of Interest
RPAS	Remotely Piloted Aircraft System
RTP	Reduced-to-Pole
SRTM	Shuttle Radar Topography Mission
THD	Total Horizontal Derivative
TMI	Total Magnetic Intensity
TTG	Tonalite-trondhjemite-granodiorite
USGS	United States Geological Survey
VTEM	Versatile Domain Electromagnetics
WGS	World Geodetic System

1 Introduction

1.1 Background

The study area is located within the Southern District of the Republic of Botswana, 55 km southwest of Lobatse (Figure 1). It is underlain by Archaean-aged rocks of the Kraaipan granite-greenstone terrane which hosts numerous gold mines and occurrences, including two notable deposits in the Republic of South Africa, namely Kalahari Goldridge mine ("Kalgold") and Blue Dot deposit (Figures 1 and 3). The Kalgold mine hosted within the KGB, approximately 55 km southwest of Mahikeng, is the most significant gold deposit within the Kraaipan granite-greenstone terrane. The mine was commissioned in December 1995 with current gold production in excess of 40,000 ounces per annum, and a current life of mine of 11 years. The Blue Dot deposit is located further south within the Amalia Greenstone Belt and has an indicated resource of 76.6 Mt at 3.2 g/t gold. In addition, there are a number of smaller gold occurrences within the granite-greenstone terrane in South Africa, including the Madibe, Muirs and Gemsbok Pan gold occurrences (Figure 11).

Despite the presence of the known gold deposits and occurrences in South Africa, only a few notable gold exploration programmes have been carried out over the KGB in Botswana. These programmes were carried out by Reunion Mining in the late 1990s; Tau Mining in the mid-2000's; Discovery Metals Limited between 2011 and 2013; and Laconia Resources between 2016 and 2018. Due to this limited amount of work: (a) the extent of the KGB in Botswana is poorly constrained; (b) the lithostratigraphy is poorly understood and (c) the gold mineralisation potential is largely unexplored.

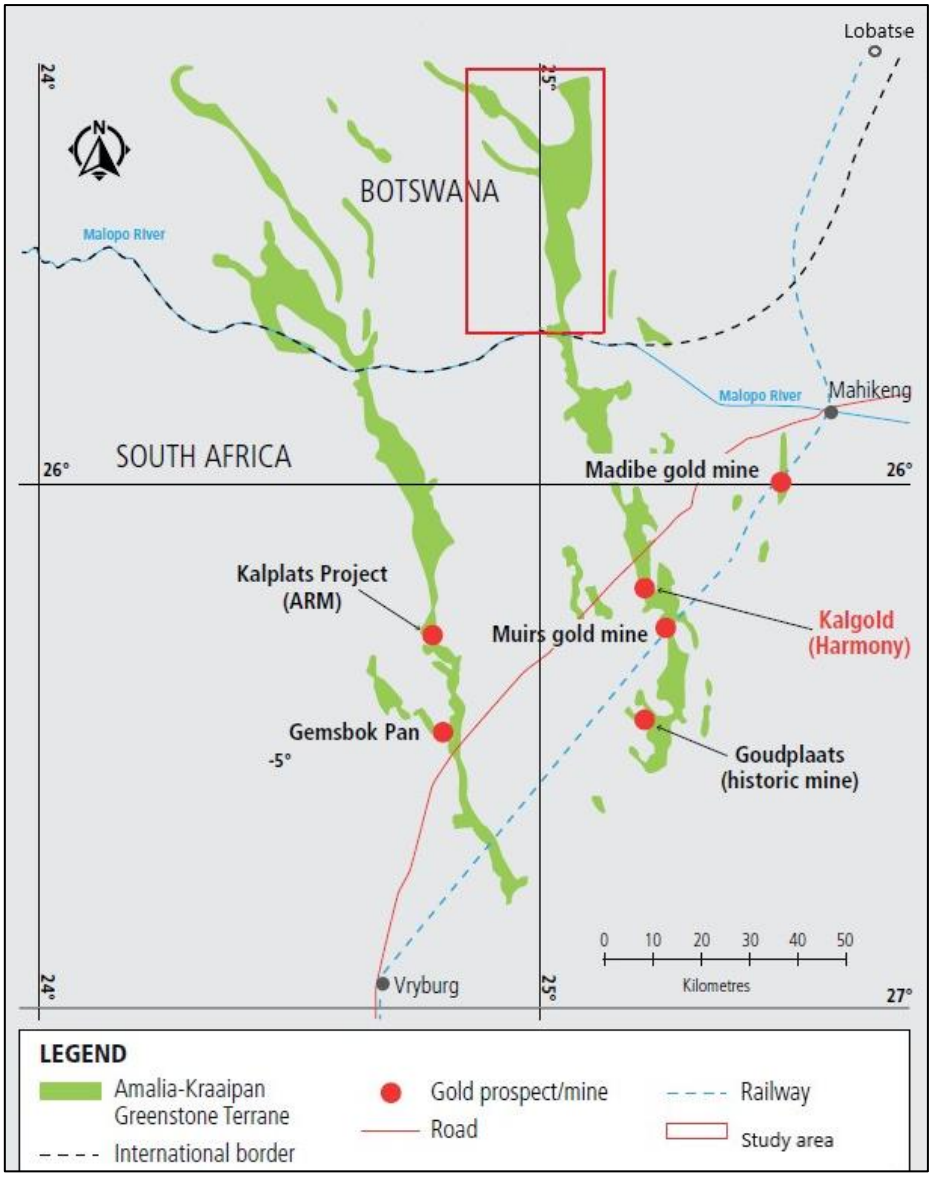


Figure 1. Locality map showing the study area relative to the greenstone belts. Modified from Harmony (2018).

1.2 Aims and Objectives

The current study is aimed at gaining a better understanding of the extent and nature of the KGB in Botswana, which is largely masked by thick and extensive Kalahari Group sediments. The same is true in South Africa, where the terrane is covered by Ventersdorp and Transvaal Supergroup rocks as well as younger Kalahari sediments. The geological unit of particular interest within the volcano-sedimentary assemblage of the KGB is the BIF, as it hosts the gold mineralisation at the Kalgold Mine. Therefore, a better understanding of this geological unit is important to determine the potential of the KGB in Botswana to host economic gold mineralisation. To that end, the following tasks were carried out:

i. Integration and interrogation of historical exploration datasets to better understand the geological, geochemical and geophysical properties of the KGB.
ii. High-resolution magnetic data was collected over an area of interest within the study area and used for detailed geological mapping.
iii. A Kalahari thickness map was created from historical exploration and water borehole datasets.
iv. Satellite imagery and remote sensing data was used for geological and regolith mapping, particularly in areas of outcrop and sub-crop.
v. An updated geological map was created with the focus on defining high-interest targets for gold exploration.

1.3 Report/Thesis Organization

Chapter 1 is an introduction to the study area. Historical work that has been conducted within the area with respect to gold mineralisation is introduced. Where gaps in understanding of the area were identified, plans have been laid out to address them. Chapter 2 summarises the regional geology of the greater Kraaipan granite-greenstone terrane as well as that of the study area. A deformational history of the area is outlined based on literature review. The geology and mineralisation of two known gold deposits within the terrane are summarised.
Chapter 3 details the methodologies which were applied in carrying out the aims and objectives of the research project. Rationales for conducting proposed work programs, and their relevance to the current research project area are explained.

The details of how the different work components of the project were conducted are presented in Chapter 4. Datasets such as drilling, geochemical data and geophysics, which were obtained from historical work programs, have been collated and interpreted to create products such as isopach maps, geochemical maps and down-hole plots. Additional data were collected during the research process through field- and desktop-based work. Chapter 5 discusses the results obtained with respect to the prospectivity of the study area for gold mineralisation. Two gold deposits that occur outside of the Kraaipan granite-greenstone terrane (and the Kaapvaal Craton at large) are presented in order that they can be compared with the study area. Potential target areas that warrant investigation within the study area have been identified. Chapter 6 presents the concluding remarks.

2 Regional Geology

The Kaapvaal Craton is endowed with large areas of granitoid gneisses which contain infolded greenstone belts or remnants thereof (Brandl et al., 2006). The most famous of the greenstone belts within the craton is the Barberton Greenstone Belt, which is one of the oldest greenstone belts in the world, and a historic gold mining district (Pearton and Viljoen, 2017). A prominent north-south magnetic feature known as the Carlsberg Magnetic Anomaly (or the Carlsberg Lineament) subdivides the Kaapvaal craton into eastern and western domains (where the latter is generally referred to as the Kimberly Block or Terrane; Figure 2). The rest of the Kaapvaal Blocks occur east of the Carlsberg anomaly and include the Witwatersrand, Swaziland and Pietersburg.

The Kimberly Block, which straddles northern South Africa and southern Botswana, hosts the Kraaipan granite-greenstone terrane (Mapeo et al., 2004 and Ramotoroko et al., 2016). The Kraaipan granite-greenstone terrane is comprised of granitoids and three sub-parallel, north-south trending greenstone belts, known from west to east as the Stella, Kraaipan and Madibe Greenstone Belt (Figures 1-3). A fourth greenstone belt, the Amalia Greenstone Belt, occurs within the Kimberly Block south of the town of Amalia (Brandl et al., 2006).

Rocks of the Kraaipan granite-greenstone terrane are incredibly difficult to study due to the fact that they are poorly exposed. The thick and extensive Ventersdorp Supergroup sequence overlies and obscures a large portion of the terrane. Younger Tertiary to recent Kalahari Group sediments in turn overlies the Ventersdorp Supergroup and the granite-greenstone terrane, obscuring it even further (Anhaeusser and Walraven, 1997; Pouljo et al., 2005; 2008; Ranganai et al., 2017). In addition to being covered, the terrane owes its poor exposure to the fact that it is generally comprised of rocks (granitoids and meta-volcanic rocks) that are prone to weathering. It has therefore been studied mainly through the use of geophysical techniques (mainly gravity and magnetics); drill-hole intersections (exploration and water boreholes); localised mining activities (particularly at the Kalgold mine) and limited field mapping from sporadic outcrops and sub-crops (riverbeds and local weathering-resistant whaleback ridges of banded iron formations).

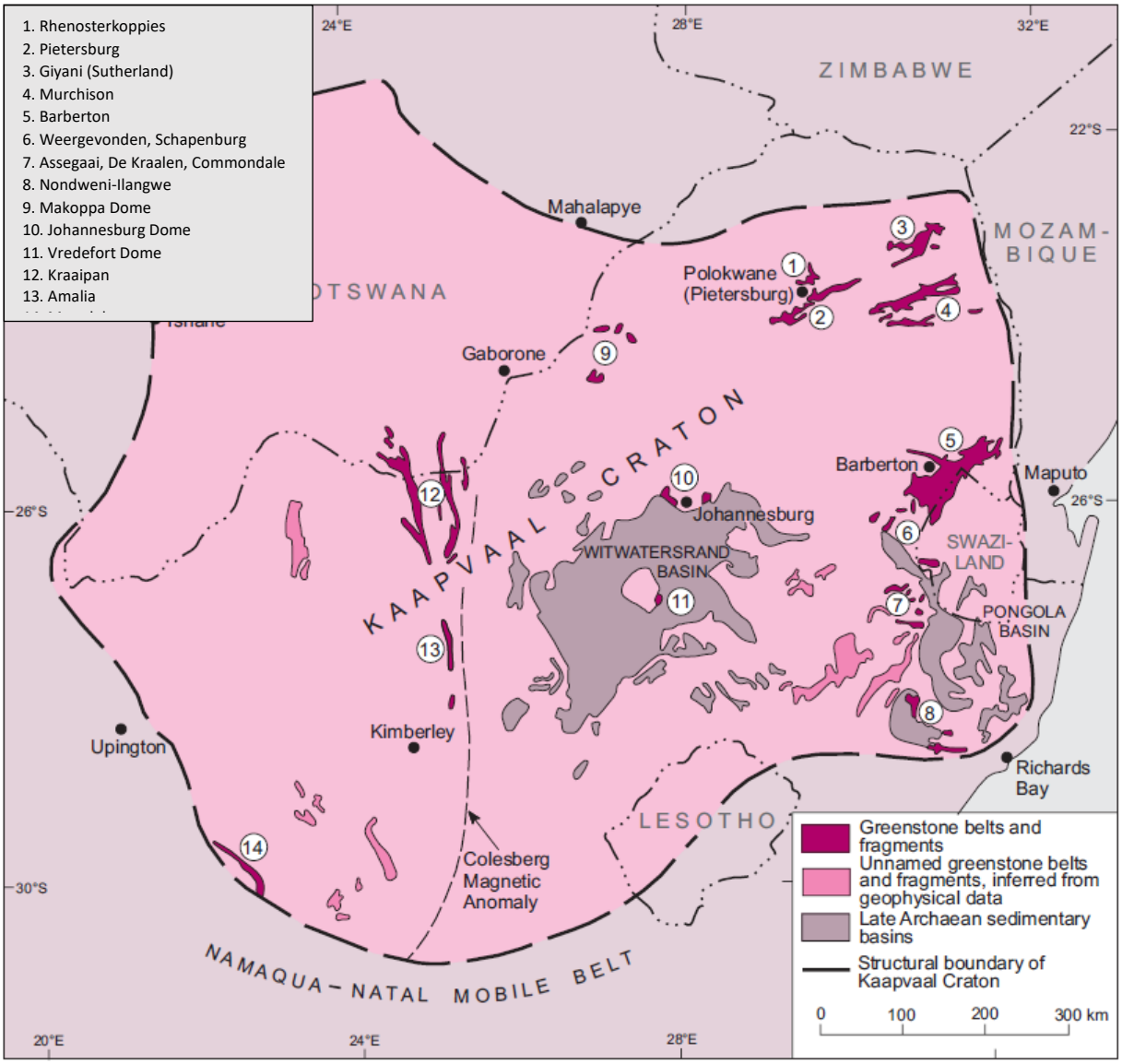


Figure 2. Distribution of the various greenstone belts and fragments on the Kaapvaal Craton. From Brandl et al., (2006).

2.1 Greenstone rocks

All of the greenstone rocks known within the Kraaipan granite-greenstone terrane have been attributed to the Kraaipan Group except for the Marydale Greenstone Belt. Poor exposure of the Kraaipan Group rocks precludes determining a definitive stratigraphic column of the succession, and thus it has been poorly recorded. Anhaeusser and Walraven (1997) mention that the most complete succession of the Kraaipan Group, which is considered the type locality, occurs north of the Kraaipan railway siding but, even there, the exposure is limited. The Kraaipan greenstone succession predominantly consists of mafic volcanoclastic assemblages interlayered with ferruginous and siliceous metasedimentary rocks. The volcano-sedimentary

succession has been categorised into three formations which occur in the following chronological order: Goldridge Formation, Ferndale Formation and Khunwana Formation (Mapukule 2009, Harmony 2019).

According to Brandl et al. (2006) the Goldridge Formation occurs at the base of the Kraaipan Group and is comprised of amphibolites (mafic meta-volcanic rocks) and associated iron formations as major constituents, while phyllites, schists and clastic sediments occur as minor constituents. The metavolcanic rocks generally display and are characterised by chlorite-actinolite-epidote alteration assemblage, typical of greenstone rocks. The iron formations consist of alternating laminae of silica rich (chert) and iron-oxide rich hematite, goethite and magnetite units.

The Goldridge Formation is structurally overlain by the Ferndale Formation, which is comprised mainly of chert that is both ferruginous and jaspillitic. The chert is interlayered with felsic volcanic rocks which are rhyolitic in composition. The Ferndale jespillites consists of cryptocrystalline quartz and poorly define magnetite layers and is not known to exist in the Madibe Greenstone Belt (Keyser and Du Plessis, 1993).

The Khunwana Formation forms the upper part of the Kraaipan Group and is apparently lithologically very similar to the basal Goldridge Formation. It consists of mafic meta-volcanic rocks whose deformation ranges from non-existent to intense (Brandl et al., 2006). The mafic-volcanic rocks display amygdaloidal textures and pillow structures, suggesting a basaltic protolith formed within a subaqueous environment. Where the Ferndale Formation is absent, the Khunwana Formation conformably overlies the Goldridge Formation, but even so, it is absent in the Madibe Greenstone Belt (Keyser and Du Plessis, 1993).

2.2 Granitoids (granites and gneisses)

The greenstone belt rocks occur in association with granitoids which were emplaced episodically into the Kraaipan granite-greenstone terrane. The intrusive relationships between the granitoids and the greenstone rocks is poorly understood due to limited exposure (Elburg and Poujol, 2020). The granitoids of the terrane occur as different varieties, all of which contain xenoliths of amphibolites and banded iron formations of the Kraaipan Group succession (Anhaeusser and Walraven, 1997). The authors concurred with previous works proposing a threefold subdivision of the granitoids, primarily based on exposure in different localities.

These include: (a) foliated leucogranites and migmatites, (b) fine to medium-grained pink or grey homogenous granitoids which are generally massive, although locally weakly foliated and, (c) coarse to very coarse-grained pink granites.

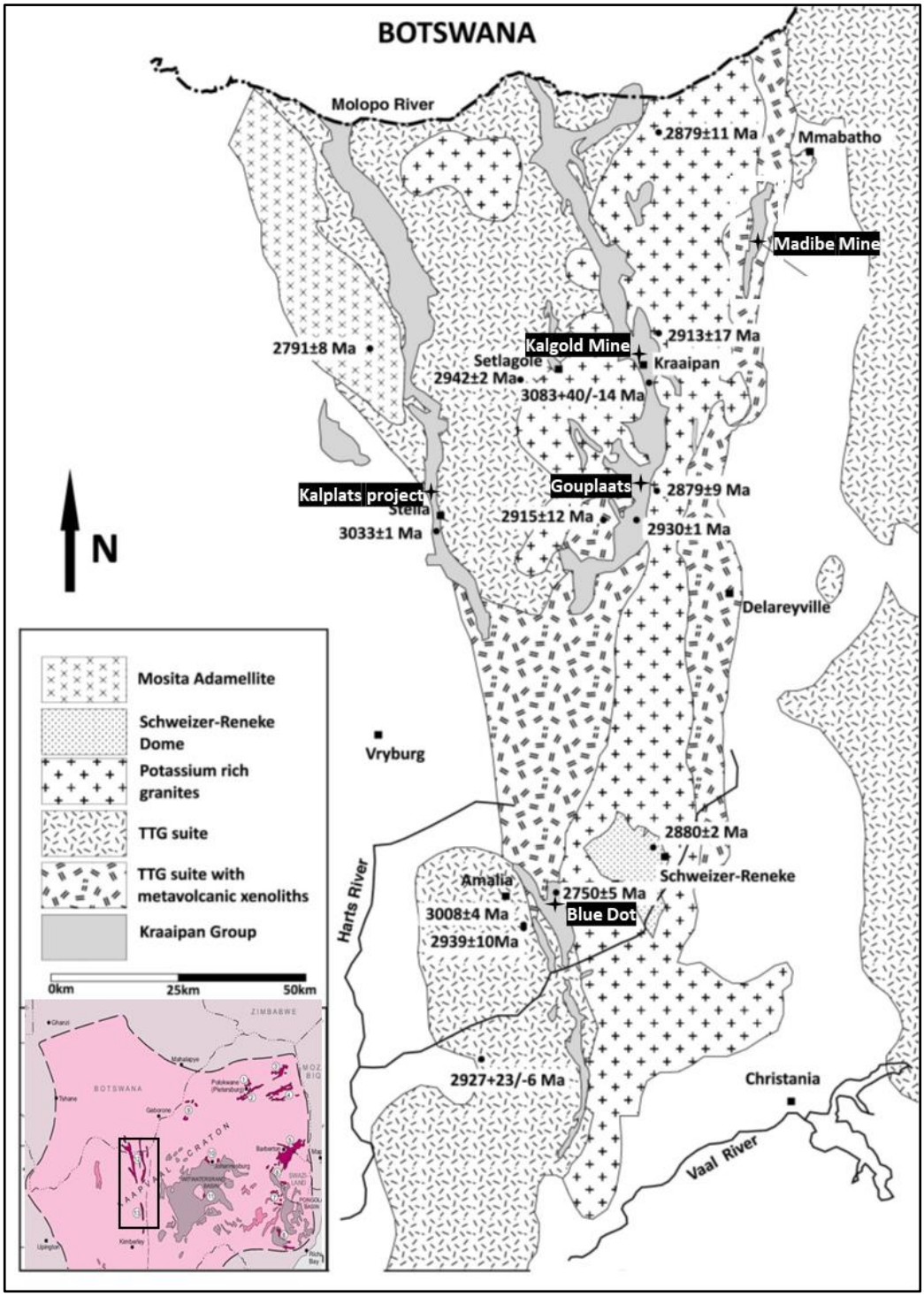


Figure 3. Generalised geological map of the Kraaipan granite-greenstone terrane within the Kimberly Block of the Kaapvaal Craton showing locations of active mines, defunct mines and gold occurrences. The overview map is a cropped version of Figure 2. Modified from Poujol et al. (2008).

The granitoids are also distinguished based on geochemical and petrological data. These were classified broadly into: (a) tonalite-trondhjemite granitoid (TTG) gneissic suite with low Na_2O/K_2O ratios; (b) K_2O-rich syenogranites and granodiorites; and (c) K_2O-rich adamellites (Figure 3). In places, the TTG gneissic rocks have been intruded by the granodiorite-adamellite suites providing an age-relationship between the two granitoids.

An age of 3008±4 Ma was obtained for the TTG suite (Figure 3), which represents the oldest known age of a granitoid within the Kraaipan granite-greenstone terrane (Poujol 2005; 2008). Ages of 2884±2 Ma and 2836±22 Ma were recorded respectively for the Schweizer-Reneke adamellite and the Kraaipan granodiorite-adamellite by Anhaeusser and Walraven (1997). The youngest granitoid within the terrane has been recorded in southern Botswana at 2782±6 Ma by Mapeo et al. (2004). This age is generally used to fix the minimum age of the Kraaipan granite-greenstone terrane.

2.3 Deformation

At least three phases of deformation, D1 to D3, have been recognised within the Kraaipan greenstone belts (Aldiss, 1985; Hammond, 2002; Mapeo et al., 2004; Hammond and Moore, 2006; Adamko-Ansah et al., 2013). D1 resulted in widespread regional deformation of the greenstones, characterised by penetrative layer-parallel foliation. All four greenstone belts within the Kraaipan granite-greenstone terrane display a similar attitude, whereby the exposed BIFs exhibit a strong penetrative fabric that is parallel to sub-parallel to the overall trend of the greenstone belts. This observation has led to the likelihood that a significant sub-parallel fault or shear zone was active during the D1 event (Anhaeusser, 1991). Hammond (2002) noted the foliation at Kalgold to be more pronounced in the phyllosilicates and carbonates, and its average orientation to be consistent with the regional trend of the greenstone belt at the mine locality. In the Amalia Greenstone Belt, Anhaeusser (1991) observed strong pervasive deformation in the exposed greenstone lithologies and postulated that this, together with the trend of the formation could be suggestive of an occurrence of a coincident major shear zone or a series of shear zones. The occurrence of a mylonitic zone and gossanous schist in the Blue Dot deposits supports this theory.

D2 was largely ductile and accompanied by crustal shortening, resulting in tight isoclinal folding; boudin formation and shearing within the BIF (Hammond, 2002). The deformation

event was for the most part not pervasive enough to cause significant re-orientation of the D1 structures. The D2 event represented the mineralising event and controlled the geometry of the lode system, which is characterized by shallow-dipping extension veins seen at the Kalgold Mine (Hammond, 2002). At the Blue Dot deposit, Anhaeusser (1991) noted that D2 may have resulted from granitic plutonism causing boudinaging of the chert-rich layers within the BIF and formation of pod-like features within it, which were subsequently mineralised at the Goudplaats Mine. D2 is likely to have transitioned to brittle deformation, resulting in extension fractures observed by Hammond (2002) at Kalgold. Aldiss' (1985) study of the deformation events at Mosi ridge in southern Botswana noted D1 intrafolial minor folds. These tight to isoclinal folds rotated during D2 such that their axial planes are oriented largely sub-parallel to the D2 foliation planes.

D3 resulted from regional extension, causing development of broad open folds with easterly dipping axial planes and localised zones of shearing/faulting (Hammond, 2002). D3 is represented by a late-stage right lateral movement which caused rotational slip; formation of NE-SW shears; formation of bedding-parallel slips; and brecciation. This late-stage brittle deformation phase was also responsible for mineralisation as these structures are enriched with sulphides and associated gold mineralisation within the BIF (Anhaeusser 1991).

2.4 Kraaipan granite-greenstone gold mineralisation

Two significant gold deposits are hosted within the Kraaipan granite-greenstone terrane, namely the Kalahari Goldridge Mine which occurs within the KGB and the Blue Dot Mine hosted within the Amalia Greenstone Belt (Figures 1 to 3). Smaller mines were also opened in the past at Madibe (approximately 20 km SW of Mahikeng, where mining ceased in the 1930's due to inconsistent gold grades after the secondary supergene enrichment zone had been depleted); Muirs Mine (immediately north of the Kraaipan siding) and at other localities (Anhaeusser, 1991).

2.4.1 Kalahari Goldridge Mine

The gold mineralisation associated with the Kalahari Goldridge deposit extends north-south along a strike of approximately 6.5 km and varies in width between 15 m and 45 m (Hammond and Moore, 2006; Hammond and Morishita, 2009) and a depth of more than 300 m below surface. The deposit is subdivided into four mineralisation zones namely, the D Zone; A Zone; Watertank and Windmill (Figure 4a). The D Zone is the largest and the most significant in

terms of gold mineralisation. The D Zone has however, largely been mined-out and production is currently active in the A Zone pit (Pearton and Viljoen, 2017). Exploration is currently underway along strike of the Kalahari Goldridge mine.

According to Hammond and Moore (2006), the geology of the D Zone is comprised of mafic schists within the footwall, which are overlain by BIFs hosting the gold mineralisation (Figure 4b and 4c). The hanging-wall overlying the BIF unit is comprised of clastic metasedimentary units (graded Bouma-cycle units commencing with conglomerate, followed by greywacke and terminating with a phyllitic cap).

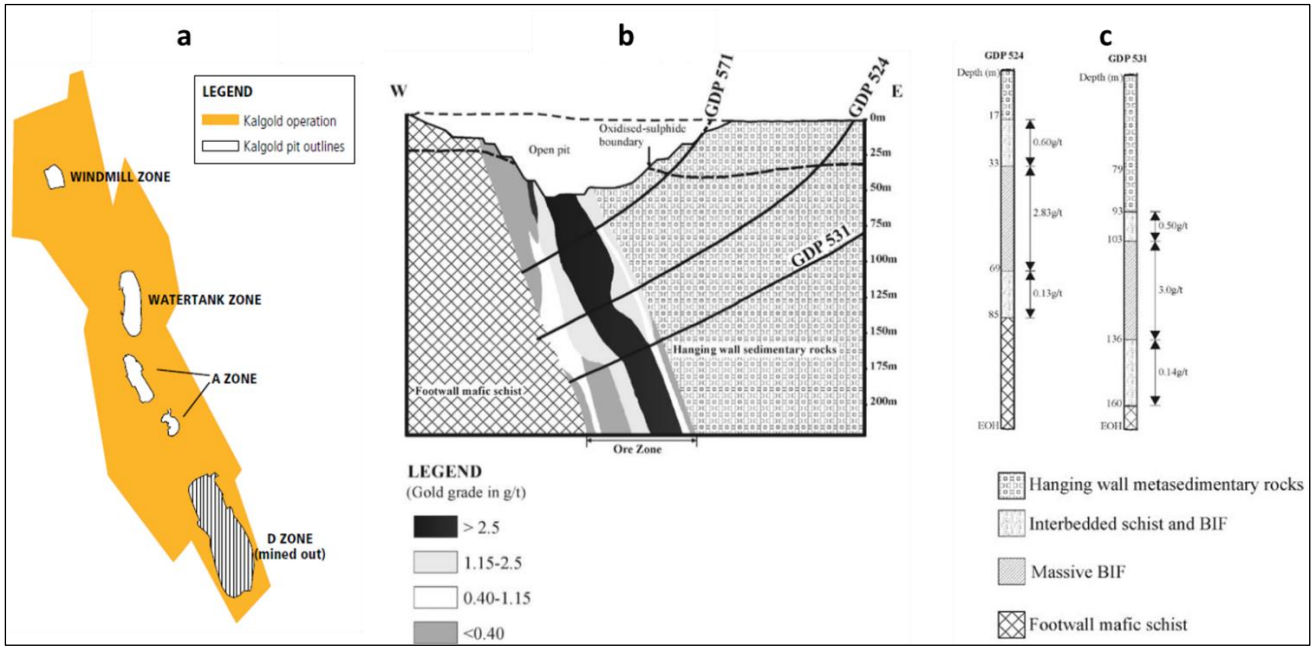


Figure 4. a) Overview map of the Kalgold deposit. b) Cross-section of the now mined-out D Zone deposit showing distribution of gold mineralisation of the orebody. c) Simplified drill-logs showing deposit lithologies and average gold grades (from Hammond and Moore, 2006).

The gold mineralisation forms a stratabound deposit hosted by the BIF unit (Figure 4b). Hammond and Morishita (2009) recognised three sets of veins at Kalgold (Group I, II and III), where Type II are confined to the BIF, and are the only set associated with gold mineralisation. Gold mineralisation is controlled by three aspects namely, lithological competency contrast, host rock geochemistry and structure.

The role of rock competency is displayed by the fact that the mineralised BIF is brecciated and is intensely veined relative to the adjacent rocks. Folds and boudins are present mainly in the

chert-rich portions of the BIF, while extension veins are present mainly in the iron-rich portions, which also suggests a brittle-ductile regime under which mineralisation occurred (Hammond 2002). High gold grades are associated with sulphide and carbonate alteration zones in the BIF, suggesting that the BIF's favourable chemistry (relatively high Fe/Fe+Mg ratio) influenced gold deposition through desulphidation of auriferous fluids (Hammond and Morishita, 2009). These authors recognised two subsets of the Group II veins (A and B; Figure 5), which are associated with mineralisation, and therefore, evidence for two separate episodes of mineralisation. Earlier Group IIA veins are ladder-vein sets localised in the iron-rich mesobands of the BIF, while later Group IIB veins are relatively thicker and laterally more extensive (up to 20 cm thick and over 20 m long).

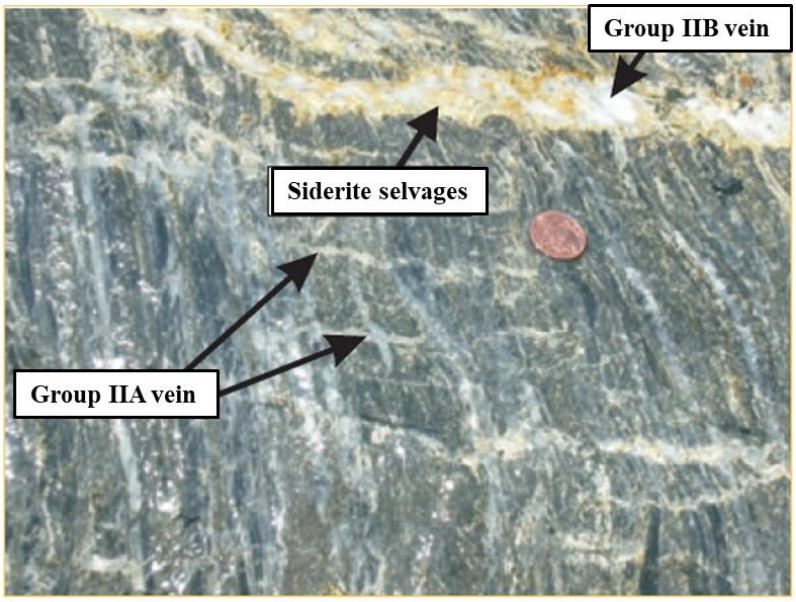


Figure 5. Group II veins occurring within the mineralised and altered BIF (after Hammond and Morishita, 2009).

2.4.2 Blue Dot Deposit

The Blue Dot deposit hosted within the Amalia Greenstone Belt (Figure 3 and 6) occurs as three distinct stratabound ore bodies near Amalia, namely Goudplaats; Abelskop and Bothmasrust (Okujeni et al., 2005; Adomako-Ansah et al., 2013; Pearton and Viljoen 2017). According to Adomako-Ansah et al., (2013) the Blue Dot deposit is comprised of BIF units which are flanked by a mafic volcanic schist and muscovite-chlorite-carbonate-quartz in the footwall and quartz-chlorite-ferroan dolomite-albite schist in the hanging wall.

The BIF units are characterised into two types: (1) the jasper-free variety which is the common BIF type in the Amalia Greenstone Belt, and (2) the quartz-carbonate-veined, jasper-rich BIF which is characterised by pyrite-hematite-carbonate-chlorite alteration (Adomako-Ansah et al., 2013). Gold mineralisation is confined to the latter sulphidised BIF, which is preferentially associated with quartz-carbonate veins. Like the Kalgold mine, the competency contrast allowed for development of dilatational sites which served as fluid conduits and loci for gold mineralisation within the BIF. Anhaeusser (1991) also references the best gold grades being concentrated in boudinaged and dismembered pod-like bodies. Chemical favourability of the Fe-rich and sulphidised BIF promoted gold precipitation from auriferous fluids (Adomako-Ansah et al., 2013), as is the case at Kalgold.

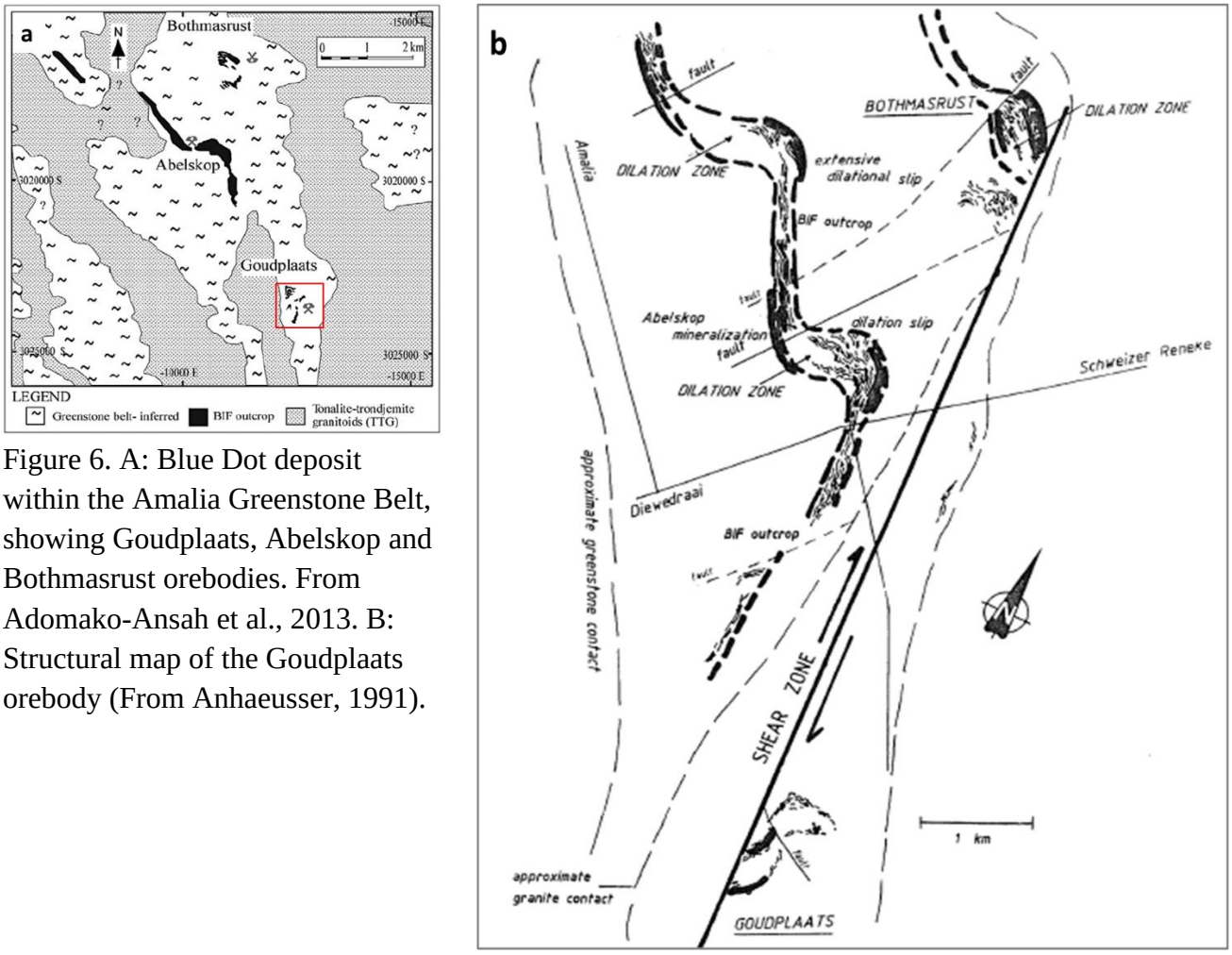


Figure 6. A: Blue Dot deposit within the Amalia Greenstone Belt, showing Goudplaats, Abelskop and Bothmasrust orebodies. From Adomako-Ansah et al., 2013. B: Structural map of the Goudplaats orebody (From Anhaeusser, 1991).

Adomako-Ansah et al. (2013) noted that gold is not solely a replacement product in magnetite-hematite rich units, because hydrothermal pyrite grains with associated gold do not show replacement textures but are in sharp contact with euhedral to subhedral iron-oxide minerals. This suggests that the re-crystallization of these oxides was in part contemporaneous with the

sulphide precipitation. They propose a magmatic source (or dissolution of rock with magmatic protolith) for the sulphides, based on estimated $\delta^{34}S_{\Sigma S}$ (= +1.8 to +2.5‰) and low base-metal / gold ratio of the deposit.

3 Methodology

3.1 Magnetic data acquisition and interpretation

Geophysical data has become indispensable for geological investigations and is particularly useful where the geology is masked by overlying cover. In this study area, the Kraaipan granite-greenstone rocks are largely covered by Kalahari sediments and can only be mapped and studied by interpreting geophysical datasets. In addition, structure, alteration and potential mineralisation can also be studied. Geophysics is also important irrespective of the scale that is desired for the mapping as the resolution can be adapted accordingly.

Magnetic data was deemed the most useful geophysical data for the study area due to the high-interest greenstone lithologies, in particular the BIF, having magnetic susceptibilities that are distinct from the surrounding granitic rocks. Magnetic data is useful for mapping lithological contacts and structure. Historical magnetic data was sourced from the Botswana Geological Institute. It was available in gridded format, with standard magnetic data filters already applied to it (i.e., reduced-to-pole "RTP" total magnetic intensity, first vertical derivative and analytical signal TIFF images). A range of magnetic responses were noticed and distinguished (low-high magnetic intensity, remanent magnetism, etc), as they represent the magnetic properties of various causative underlying rock formations. The different magnetic data filter products were also useful for identification of geological contacts and delineation of structural features such as rock fabric, zones of displacement and discordant intrusive rocks.

The historical airborne geophysical data was collected at 250 m line-spacing and is therefore considered to be low-resolution by modern standards. A portion of the study area was selected for the acquisition of high-resolution magnetic data. This area forms the north-eastern extension of the KGB in Botswana, and the survey was flown to accurately map the underlying greenstone belt lithologies and associated structural features. The data was collected using a magnetometer-mounted RPAS (remotely piloted aircraft system). The survey was flown at 25 m line-spacing at a survey height of approximately 30 m. Various magnetic data filters were used to discern differences in magnetic responses as much as possible.

3.2 Kalahari isopach map

The geology of the study area is generally masked by Kalahari Group sediments (unconsolidated sand and duricrust). It is imperative to constrain the Kalahari cover thickness (i.e., depth of burial of the strata of interest) in order to (a) decide which geophysical exploration techniques would be effective within the study area; (b) design optimal geochemical sample collection and analytical; and (c) determine the most effective drilling techniques for testing high-interest targets.

Historical water and exploration borehole databases were sourced from the Botswana Geological Institute and press releases from both public and private companies. The bulk of the boreholes were from water drilling programmes containing very little geological information. Therefore, only a few of these holes were useful in determining the Kalahari thickness. For areas where the sub-Kalahari rock exposures are known to exist (such as the BIF outcrops), additional "dummy" boreholes were created and designated zero Kalahari depth. The increased datapoint density helped to improve the accuracy of the cover thickness map. Boreholes were plotted spatially in QGIS, and the contouring plugin of the programme used for generating contours of the Kalahari cover Kalahari isopachs.

3.3 Photogeology and Remote Sensing

Geological and geomorphological mapping has always benefited greatly from the use of aerial photographs. Accurately positioned, high-resolution satellite imagery (orthophotos and remote sensed data) plays a pivotal role in regolith and lithological discrimination.

The SAS Planet application makes it possible to download satellite imagery from a wide selection of maps supplied by services such as Google Earth; Bing Maps; ESRI; Yahoo Maps; etc. The imagery can be downloaded at a desired resolution, based on a zoom level defined by the user. Many output formats are available for the images and include Joint Graphic Expert Group "JPEG", Enhanced Compression Wavelet "ECW", Portable Network Graphics "PNG", etc. The application offers a built-in facility to stitch together different image tiles for the selected area of interest such that the output is a single complete file. An appropriate projection system can be set for the output image such that it plots correctly within the geographical area of interest. For the study area, an ECW format satellite image was downloaded from the application, set at the WGS1984 Geographic projection system. This satellite imagery was used

for mapping BIF, where it is exposed within the study area. Aerial photographs were used previously for mapping; however, they were generally of poor resolution and colour-rendering was not possible, which limited the enhancement of high-interest features.

In addition, freely available Landsat-8 data was downloaded from the USGS Earth Explorer website. The sensors on the Landsat-8 satellite collect data at eleven frequency windows (bands 1 to 11) along the electromagnetic spectrum (USGS). Data images for bands 1 to 7, all of which have a resolution of 30 m, were downloaded for the purposes of this study as they are the most useful for characteristic reflectance curves for most rocks and minerals. Band 8 has a different surface resolution from bands 1-7; band 9 is useful for cirrus cloud detection while 10 and 11 are useful for providing accurate surface temperatures (USGS).

A suitable scene covering the study area was chosen and images for bands 1-7 were downloaded. As part of pre-processing, the images were clipped to retain the area of interest and then subjected to the process of atmospheric correction to remove the effect of scattering and absorption of spectra by atmospheric elements. Various band combination and band ratioing techniques were applied to the data as part of image processing. Both of these techniques are routinely used for identifying and enhancing spectral differences in rocks, rock-forming minerals and other geological features. Interpretation of the band combinations and ratios involved identification of spectral differences and assigning them different land cover classes (or “training sets”), and where possible, the training sets were attributed to known geology and regolith of the area of interest. The training sets were applied in supervised classification and generation of thematic maps.

3.4 Geological field mapping and ground-truthing

Geological field mapping was carried out in areas of outcrop, which were identified from satellite imagery and topographic data (digital elevation model). No regolith mapping was possible in the field other than differentiating outcrop-scree surrounding from Kalahari sand cover.

A hand-held GPS (Garmin GPSMAP 64s) was used for navigation and marking of waypoints of interest. A Brunton geological compass was used for collecting structural measurements, including foliations, lineations, joints, faults and folds. The compass gave unreliable structural

measurements (strike and dip/directions) in places where the BIF were relatively more magnetic. Structural measurements were recorded using the Clar notation (i.e., a representation of structural measurements as dip direction over dip angle, consistently in three and two digits respectively; therefore, a feature with a measurement 045°/30° dips to the northeast at 30 degrees). A magnetic declination of roughly -17 degrees for the study are was taken into account.

4 Historical data review

The earliest geological programmes over the study area were conducted by Billiton Botswana during their exploration initiative for Cu-Ni deposits (Carney 1994 and Reunion Mining 1999). Their regional magnetic survey data, collected at 250 m line-spacing in the early 1980s, helped to improve the geological understanding of the area. The magnetic data, together with drill-hole information from water drilling and other mineral exploration efforts significantly improved the geological understanding of the study area. Although the Kraaipan Group rocks in the area were known for a long time due the outcropping BIF ridges, the understanding improved significantly between 1996 and 1999 when Reunion Mining Botswana (Pty) Ltd (Reunion Mining 1999) carried out various exploration programmes. Their interest to explore the Kraaipan Greenstone Belt was awakened by the discovery of the Kalgold deposit in South Africa. Historical datasets collected during the above-mentioned works were collated and assessed with data collected during the current study in order to gain a better understanding of the geology of the area and to identify areas of potential interest for gold exploration.

4.1 Geophysical survey data

Magnetic data is the most widely available geophysical data within the study area. Most of it is historical regional data that was collected at 250 m line-spacing or wider (Carney 1994) and is therefore low-resolution. Even so, this data has been used successfully in mineral exploration and other investigative geological campaigns to outline the nature and extent of the Kraaipan greenstone rocks. These are easily distinguishable from surrounding granitic rocks due to their relatively strong magnetic susceptibilities. Maps in Figure 7 depict the reduced-to-pole and first vertical derivative images of the magnetic data, where the north-south oriented high amplitude linear magnetic responses correspond to the BIFs and associated greenstone rocks.

Discontinuities and displacements are observable along the trend of the greenstone rocks and in most cases, they are clearly associated with NW-SE oriented faults. Two additional sets of interpreted faults can be depicted from the magnetic data; that which is trending parallel to the BIF as well as the SSE-NNE set which is parallel to the prominent rock fabric (Figure 7b). Intrusive linear magnetic dykes are also mappable from the regional magnetic data (Figure 7a and b).

There are ambiguities with respect to the northern extent of the KGB and the exact location of the contact between it and the younger Transvaal Supergroup rocks in southern Botswana. Others have interpreted the belt to form an arcuate shape towards the northern extremity, branching into the area outlined by the white polygon in Figure 7.

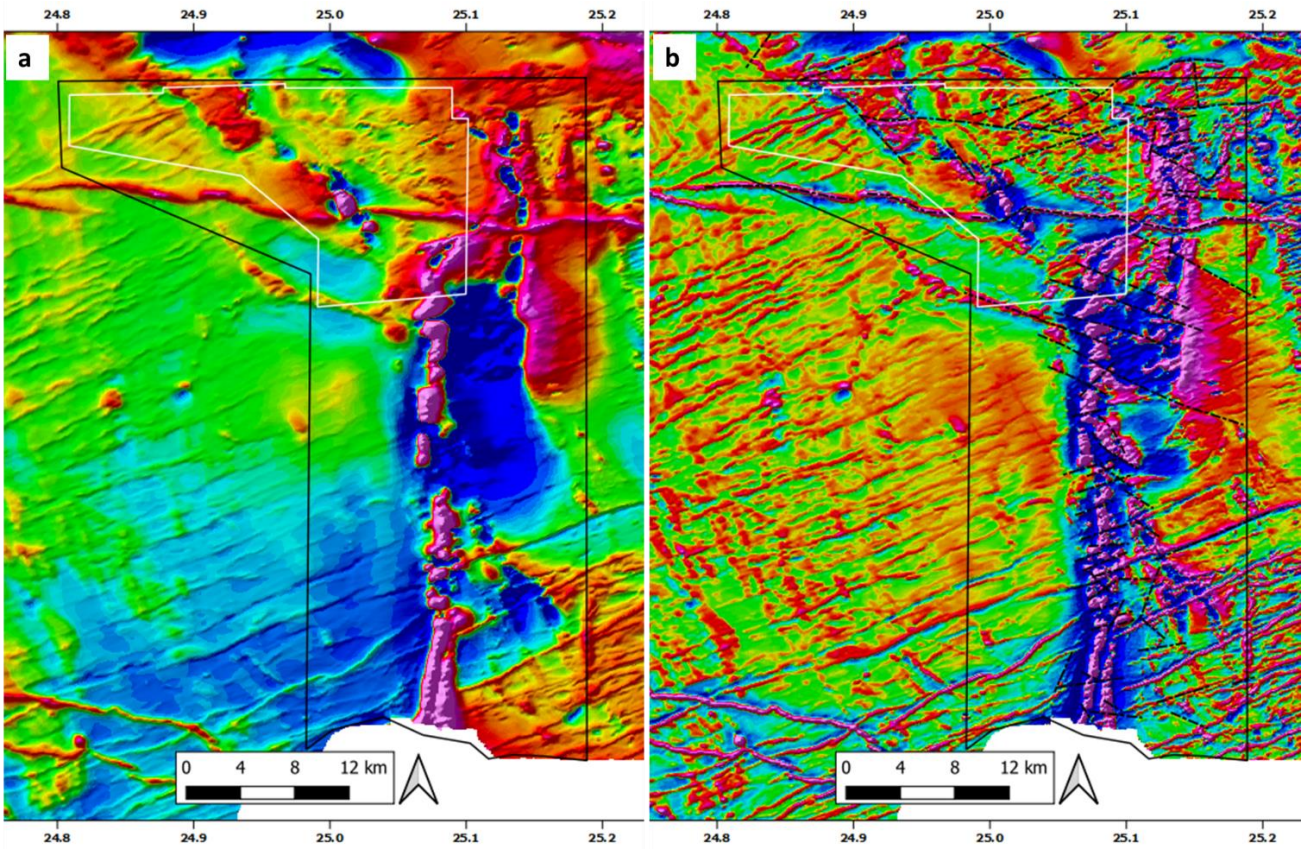


Figure 7. Images of regional magnetic data collected at 250 m line-spacing or wider. A high-resolution magnetic survey was conducted within the area outlined by the white polygon. A: Reduced-to-pole "RTP" image of total magnetic intensity. B: First vertical derivative of RTP, where dashed black lines show interpreted faults. The black polygon outlines the study area.

A high-resolution magnetic survey was conducted over this area at the resolution of 25 m spaced north-south grid lines, 200 m spaced east-west tie-lines and a sensor height of 20 m. The magnetic data was collected using a fixed-wing remotely piloted aircraft system (RPAS) which is mounted with a Gem GSMP-35A high-sensitivity magnetometer. This survey is by far of the highest resolution to ever be conducted on the Botswana sector of the KGB. The aim of the survey was to; (I) confirm the presence of the Kraaipan greenstone rocks within the surveyed area; (II) map the structures; (III) map the accuracy of the lithological contacts and structural features based on different magnetic responses; (IV) use other geological datasets to

assign different magnetic signatures to lithological units and; (V) to investigate whether litho-structural mapping can provide further clues on deformation history of the area.

Standard filter/derivative products were produced from the total magnetic intensity (TMI) data, including; RTP-TMI (reduced-to-pole total, Figure 8a), THD (total horizontal derivative); FVD (first vertical derivative, Figure 8b) and AS (analytical signal). These derivative products were extremely useful in mapping of geological units and associated geological structures (Figure 8c).

Different magnetic intensities are distinguishable from various filters of the survey data, and they likely represent various lithological units. They ranged from magnetic lows to highs (cold to warm colours respectively, including remanent magnetisation) and have been mapped accordingly (Figure 8a to c). At least three sets of interpreted faults were observed; trending NNW, ESE and NE. Cross-cutting relationships amongst these sets of faults suggest that they formed during three separate stages of deformation, in that chronological order. The NNW set is restricted to the intermediate to highly magnetic rocks and is parallel to the regional trend. The other two sets are ubiquitous. Lateral displacement is observable along both of these sets, and in both cases the sense of movement is sinistral. The NE set is the most prominent of the interpreted fault sets and is parallel to the regional fabric.

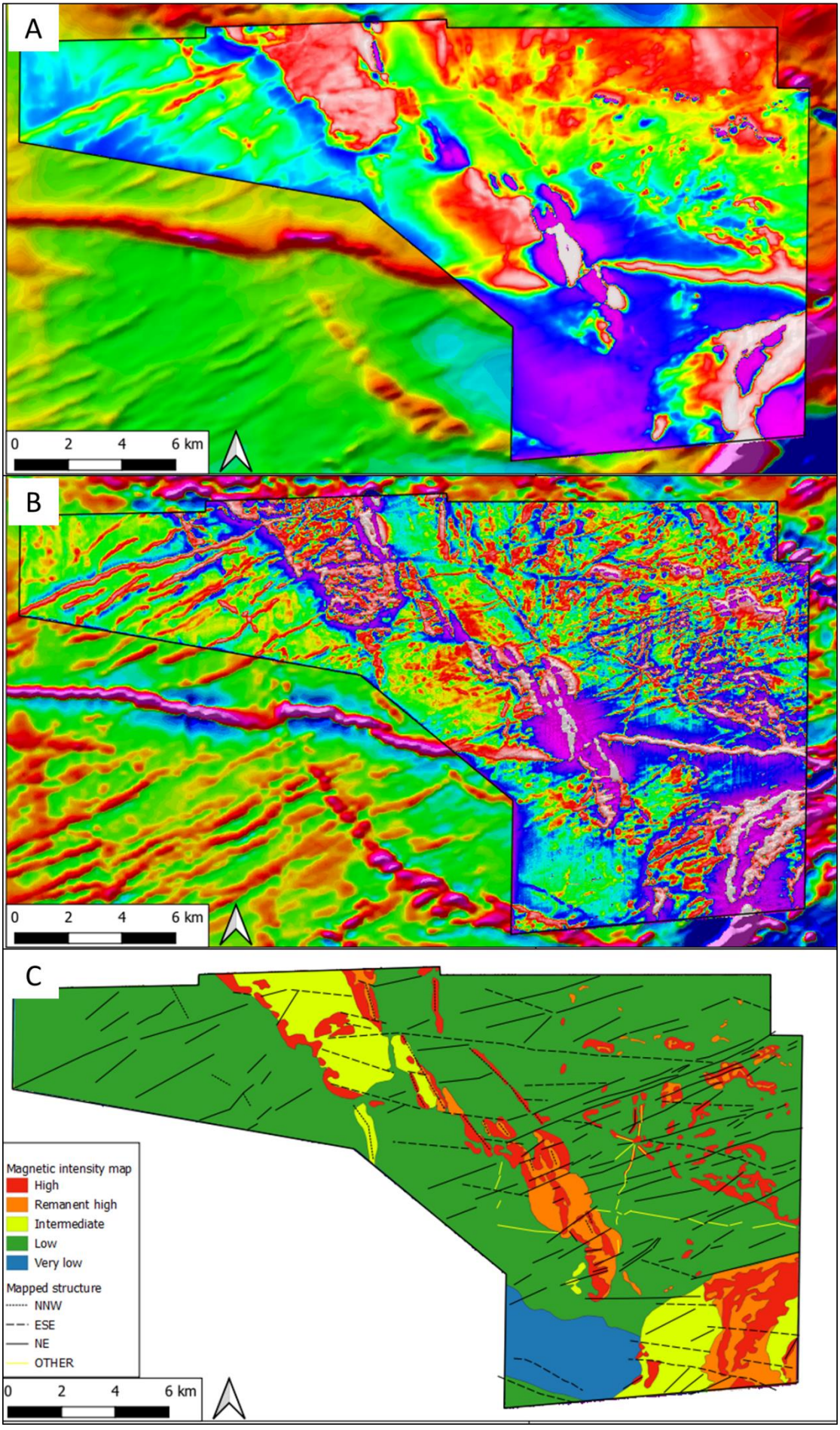

A
0 2 4 6 km
B
0 2 4 6 km
C
Magnetic intensity map
High
Remanent high
Intermediate
Low
Very low
Mapped structure
NNW
ESE
NE
OTHER
0 2 4 6 km

Figure 8. A: Reduced-to-pole image of total magnetic intensity. B: First vertical derivative image of RTP. C: interpretation map constructed from various magnetic data filters to display zones of various magnetic susceptibilities as well as different sets of faults.

4.2 Kalahari isopach mapping

The term "Kalahari cover" is here used to refer to the sedimentary deposits that are the same age or younger than the Kalahari Group sediments of southern Africa. The exact timing of initial deposition of the Kalahari Group sediments is unknown but the maximum age is fixed by the underlying Late Cretaceous kimberlite pipes (Haddon 2005). "Kalahari Group sediments" here does not refer to, and should not be confused with the sediments of the Botswana sub-basin of the Karoo Supergroup, sometimes referred to as the "Kalahari Karoo basin". Within the study area, the most common Kalahari sediments include unconsolidated sand, duricrust (mainly calcrete and silcrete), poorly consolidated sands and gritty to pebbly and poorly compacted basal gravels.

For any given area that is of interest for mineral exploration, it is always imperative to have an understanding of the nature and thickness of the Kalahari cover. The cover directly influences the choice of exploration techniques that need to be applied to an area of interest, regardless of the mineral commodity of interest.

From a geochemical soil sampling perspective, samples derived from areas of relatively thin cover would be regarded as more representative of the underlying geology (lithology, alteration and mineralisation) as opposed to those collected in areas of thicker cover. Where the cover is thick and also transported, samples are unlikely to be representative of the underlying geology. Therefore, subtle mineral-in-soil anomalism in areas of cover should be interpreted with care as the difference between background and anomalous values are expected to be low in these environments.

Similarly, geophysical surveying and remote sensing methods have limited effectiveness in areas of thick cover, and field mapping of geology is completely precluded in areas of any cover. In addition to constraining cover thickness, understanding the nature of the cover is similarly important. A geophysical magnetic survey targeting subtle magnetic features of rock units underlain by ferruginous cover is likely to be ineffective. Geochemical soil sampling in

areas of thick impermeable duricrust such as silcrete (which restricts upward and downward ground water percolation), is less effective compared to areas of unconsolidated cover.

The thickness and nature of the Kalahari cover can directly determine the financial feasibility of an underlying mineral deposit, with marginal mineral deposits becoming more challenging and costly to mine under areas of thicker cover.

The nature and thickness of the Kalahari cover within the study area was investigated by collating historical borehole datasets. Over areas of known outcrop determined from satellite imagery and field mapping excursions, "dummy" boreholes were generated and designated zero Kalahari cover thicknesses (Figure 9).

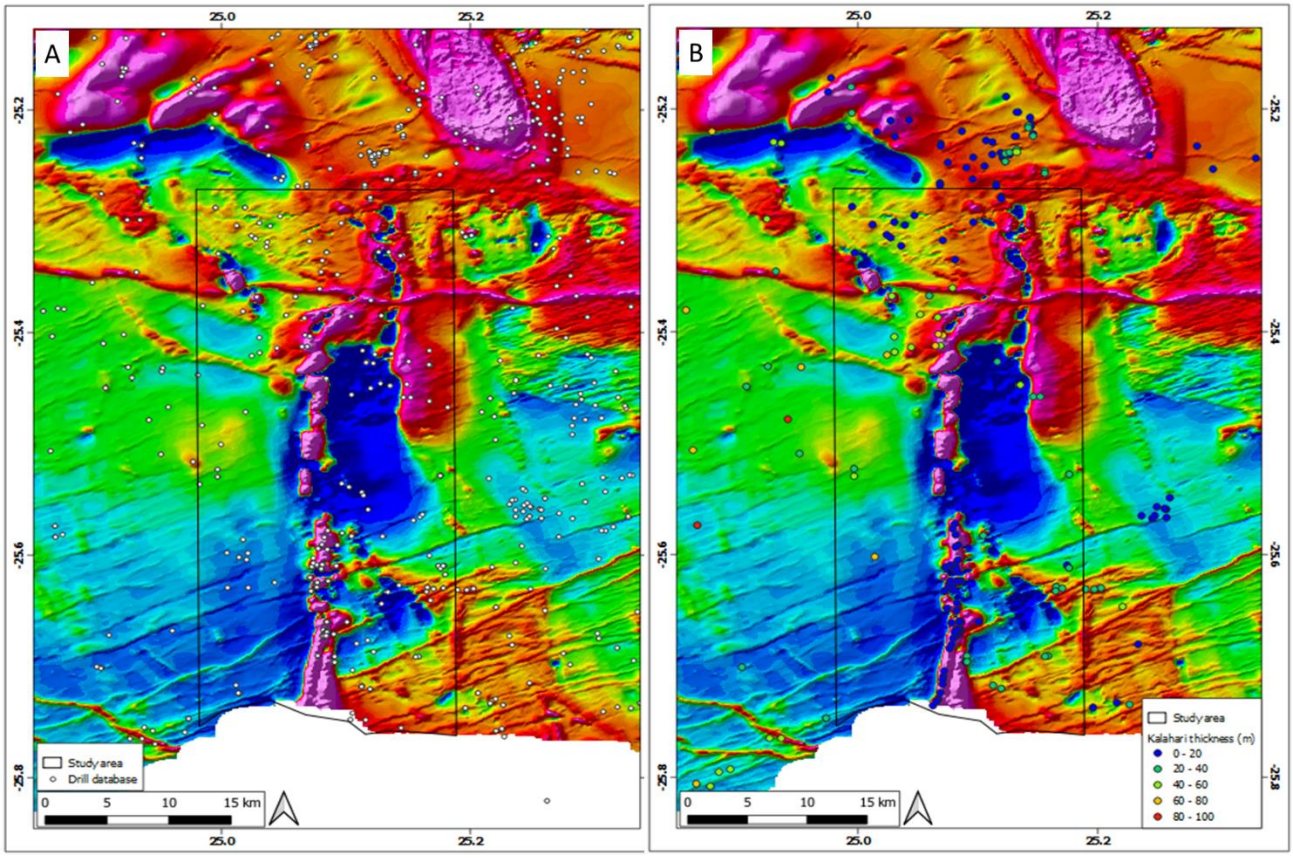


Figure 9. Location maps of drilled boreholes underlain with an RTP (reduced-to-pole) magnetic data image. (A): historical boreholes drilled within and in the vicinity of the study area. (B): boreholes with indicated Kalahari cover thicknesses, including "dummy boreholes" with zero Kalahari thickness where rock exposures are known to occur.

A Kalahari isopach map was constructed in QGIS by means of contouring the Kalahari sediment thicknesses (Figure 10). The accuracy of the isopach map was negatively influenced

by the unequal spacing between boreholes; limited availability of cover thickness information from historical water boreholes; and the reliability of historical exploration datasets.

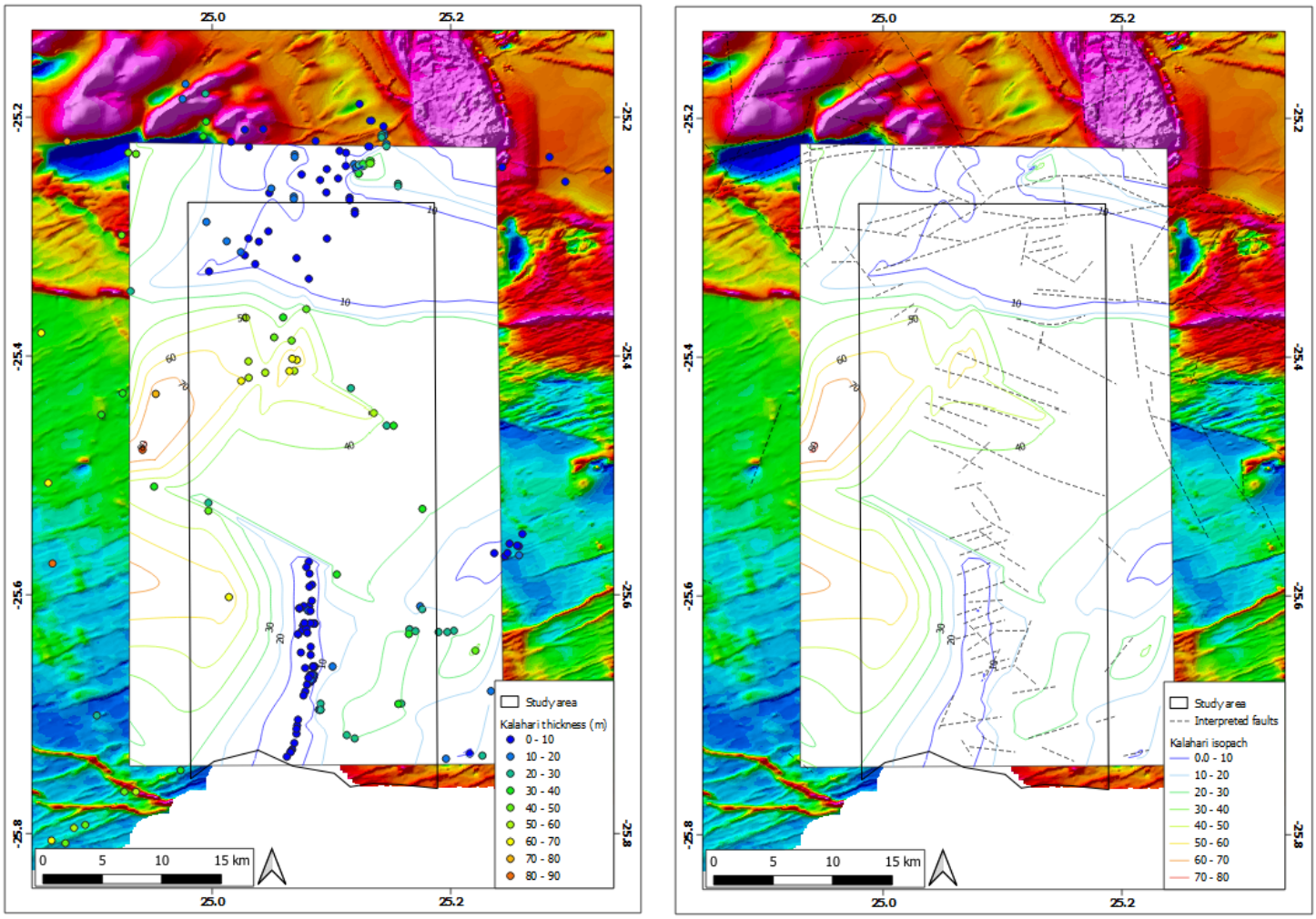


Figure 10. Constructed Kalahari isopach maps. Left: isopach contours as well as boreholes from which they were created. Right: interpreted faults overlain on Kalahari isopachs. The structural architecture seems to have greatly controlled the pre-Kalahari surface.

4.3 Geological mapping

4.3.1 Satellite imagery and remote sensing

Two types of satellite imagery were used to map surface morphology and geology, namely Bing orthophoto and remote-sensed Landsat 8 imagery. The imagery was used to determine whether the reflectance signature of the outcropping BIF and associated greenstone lithologies could be traced under cover.

Colour-rendering of the Bing orthophoto was carried out in QGIS in order to produce an image that best displays different surface features, most importantly the known BIF outcrops as well as other geomorphological features (Figure 11a to c). The ridges of linear BIF are mappable using the enhanced imagery, owing to their prominent rusty colour which has developed from iron oxidation. Locally, large structural features such as folding and faulting were observed and mapped with reasonable accuracy. These were observed as localised depressions or low-relief features within the outcropping BIF. The dark-brown colour associated with iron staining drops abruptly against the outcrops, suggesting that the BIFs have either a limited lateral extent; are steeply dipping; the lithological contacts between the BIF and adjacent rocks are sharp; or the Kalahari cover thickens rapidly away from the outcrops.

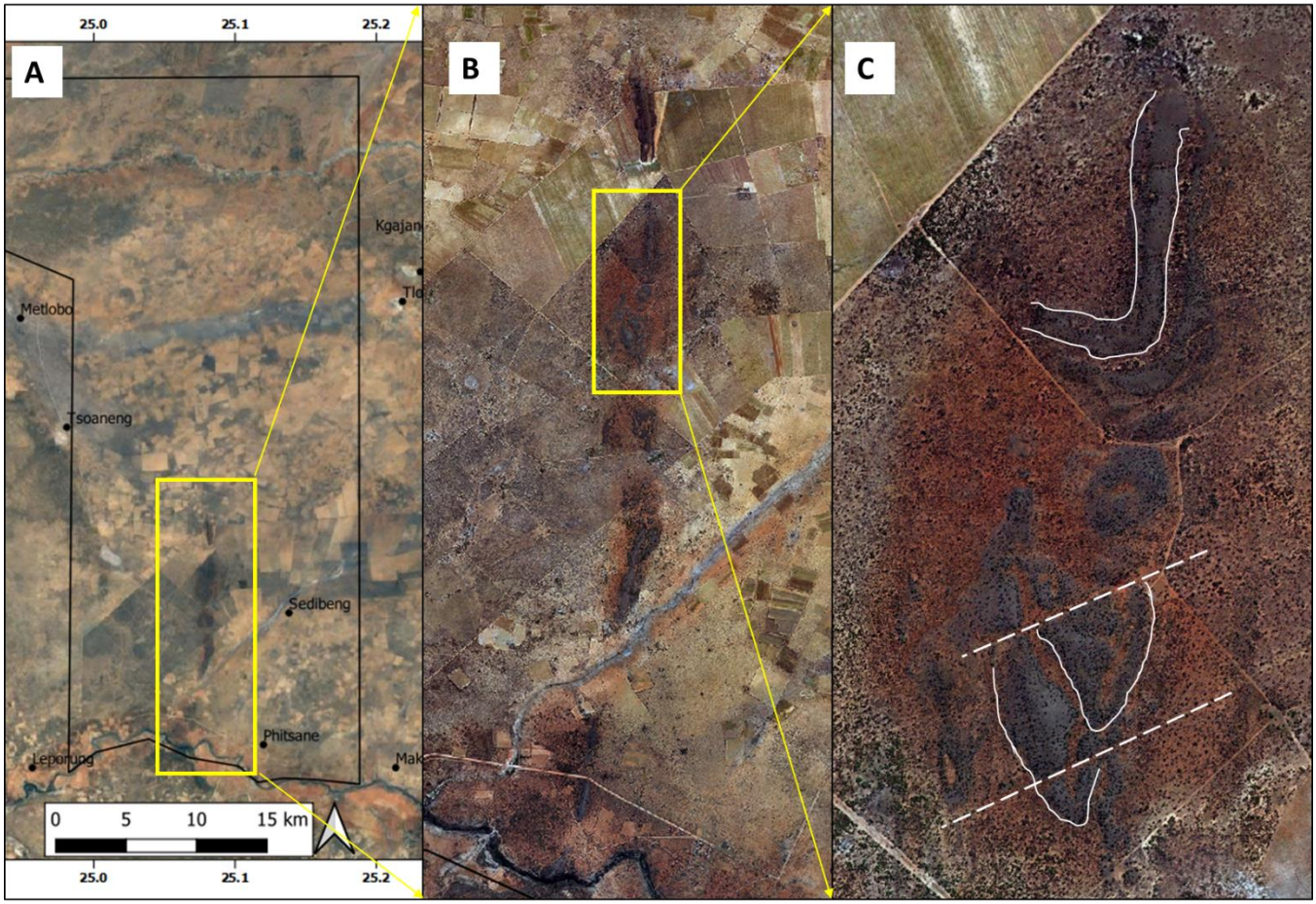


Figure 11. (A): Bing satellite image with BIF outcrops in the central southern portion of the map as a dark rusty colour. (B): enlarged area with the linear BIF outcrop. Areas of outcrop discontinuities most likely represent presence of underlying structural disruptions. (C): enlarged portion of BIF whereby folding and faulting are clearly visible from high-resolution satellite imagery (solid lines = rock fabric; dotted lines = possible faults).

Geomorphological features are also distinguishable, such as rivers (running west-east), ploughed farmland and land that is free of agricultural activity; all of which are important observations and considerations for planning exploration programmes and interpretation of exploration results.

Landsat 8 imagery was sourced from the USGS Earth Explorer website, and only images for bands 1 to 7 were chosen for the purpose of this study. The purpose being to detect greenstone belt lithologies, particularly the BIF as it is the target for gold mineralisation in the current geological setting and outcrops in places, thus increasing the chance of it being detectable in areas masked by cover. Landsat 8 bands 1 to 7 have the same resolution of 30 m (i.e., one pixel of the image covers a 30 m by 30 m area on the ground), while the rest of the bands are at different resolutions, and importantly, reflectance properties for most rock-forming minerals are detected within the wavelength of those bands (0.43 to 2.29 μm, i.e., visible light to shortwave infrared of the electromagnetic spectrum, USGS).

Spectral signatures of various objects can be highlighted from Landsat imagery by way of combining or ratioing of certain bands. The most common band combinations for Landsat 8 data include the natural colour composite (i.e., bands 5-4-3 of the visible spectrum, which displays the natural colour of the earth as humans see it, Figure 12a); short-wave infrared (bands 7-6-4, useful for displaying vegetation and vegetation density in shades of green, Figure 12b).

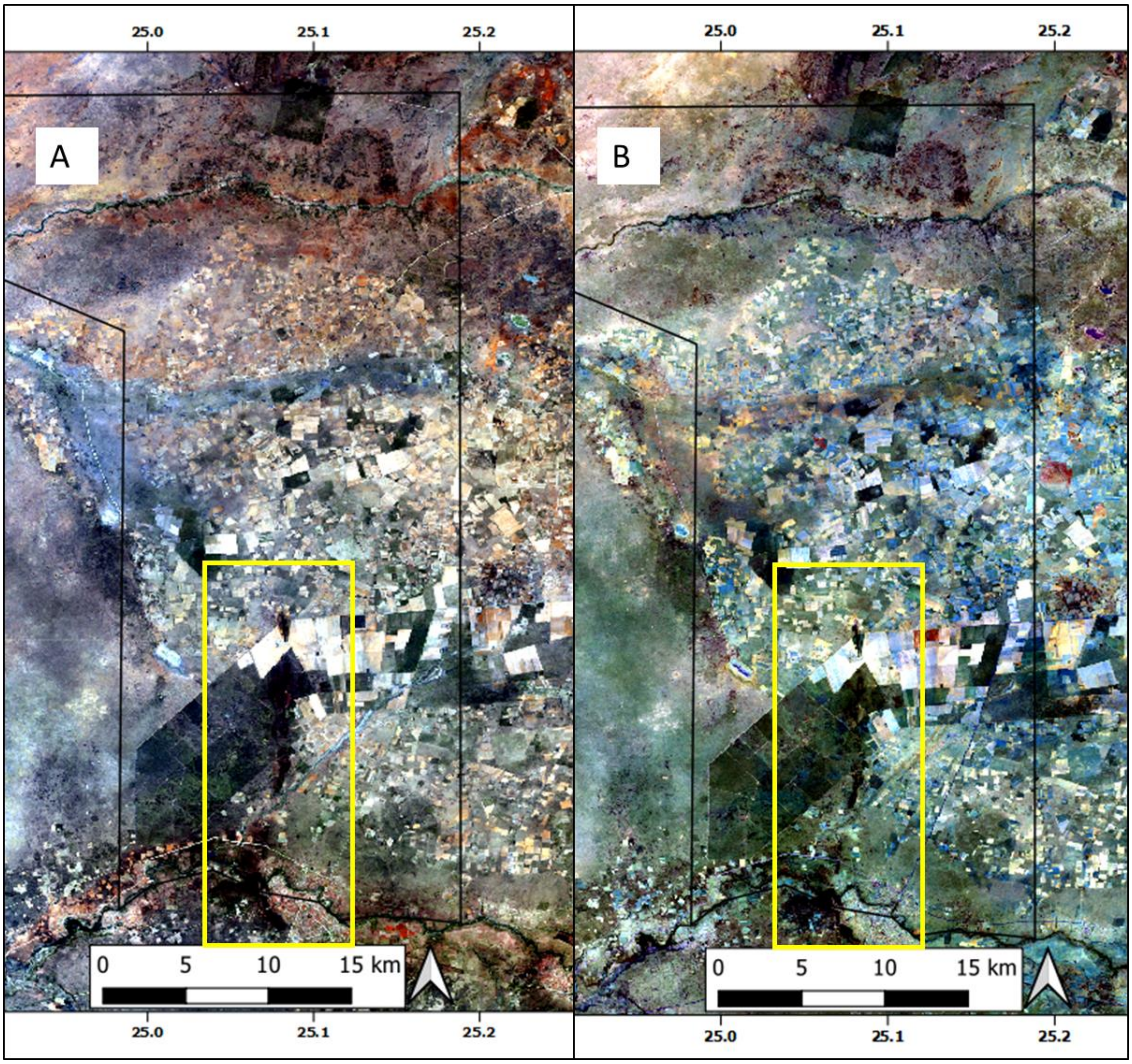


Figure 12. Landsat-8 colour composite images, where the linear north-south BIF outcrop occurs within the yellow outline. (A): true colour composite (bands 5-4-3). Rusty colour occurs on areas with Fe-rich rocks and river drainages. (B): vegetation composite (or short-wave infrared of bands 7-6-4) where the presence and density of vegetation is proportional to the intensity of the shade of green.

The USGS has developed a library of spectral reflectance curves for a wide range of minerals, and these are commonly used in geological investigations for distinguishing types of regolith and rocks. Band ratioing (which is a division of digital numbers of one band by corresponding numbers of another band) is particularly helpful for enhancement of subtle differences between selected bands (i.e., amplification of variations in slopes of the different spectral curves).

For example, Figure 13 depicts the spectral curves from Landsat 8 data for iron-bearing oxide minerals hematite, goethite and jarosite. All of these minerals display high reflectance in band 5, while spectral absorption is a characteristic for all of them in band 4. A spectral band ratio

of 5/4 therefore results in an amplification of the occurrence of these iron oxide minerals in the resultant ratioed image. Another band ratio which is commonly used for highlighting the occurrence of iron minerals is ratio 3/1, otherwise known as the iron ratio. Iron minerals typically have low reflectance in band 1 as opposed to strong reflectance in band 3 (Figure 13), resulting in high ratio values for areas with iron-bearing minerals.

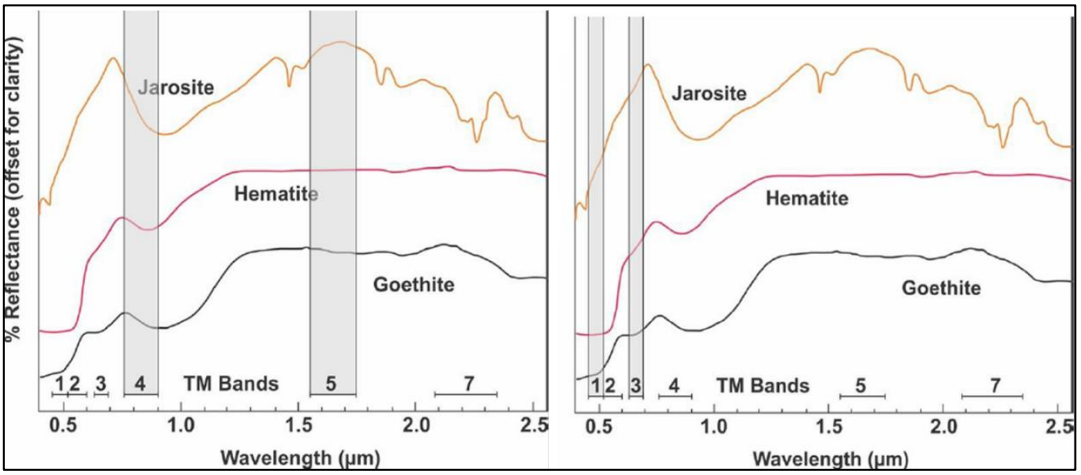


Figure 13. Spectral reflectance of jarosite, hematite and geothite (from the USGS Spectral Library). Band ratios 5/4 and 3/1 are good for enhancing spectral reflectance iron-oxide and iron-bearing rocks respectively.

Polygons were used to outline and categorise certain surface features such as rock outcrops, different soil types and vegetation cover distinguishable from band combinations and ratios, commonly referred to as land classes, themes or regions of interest “ROIs”. The resultant map displays all the themes known as a thematic map. A QGIS plugin called “Semi-automatic Classification Plugin” allows for supervised classification of remote sensing images. It was applied to the band 1-7 multispectral data for supervised classification, whereby the input ROIs were used as training sets in order to detect areas of similar spectral signatures in the multispectral data and separate those areas into different classes. Figure 14 depicts a thematic map which was generated through supervised classification.

The ROIs which were applied for supervised classification were ground-checked during field reconnaissance in order to reduce ambiguity in the supervised classification process. However, the results obtained after the classification process (i.e., extrapolation of the ROIs) cannot be said to be free of inaccuracies. It should be noted that ROIs which represented rock outcrops are BIF, Upper Transvaal 1 and 2 and Kanye Fm. BIF, which is the Kraaipan BIF, is the only

outcrop of the ROI that is present within the study area. Upper Transvaal Supergroup rocks and Kanye Formation volcanic rocks are present and outcrop in the vicinity of the study area, to the north and northwest. The classification of these rock units within the study area most likely reflect the provenance of the blanketing Kalahari cover rather than the underlying sub-Kalahari geology, even if these rocks happen to be the ones overlain by the cover, unless the cover is very thin. Rock classifications which occur distant from areas of outcrop are likely to be errors in computation. However, some of these are located proximal to drainages, which would suggest transportation by water.

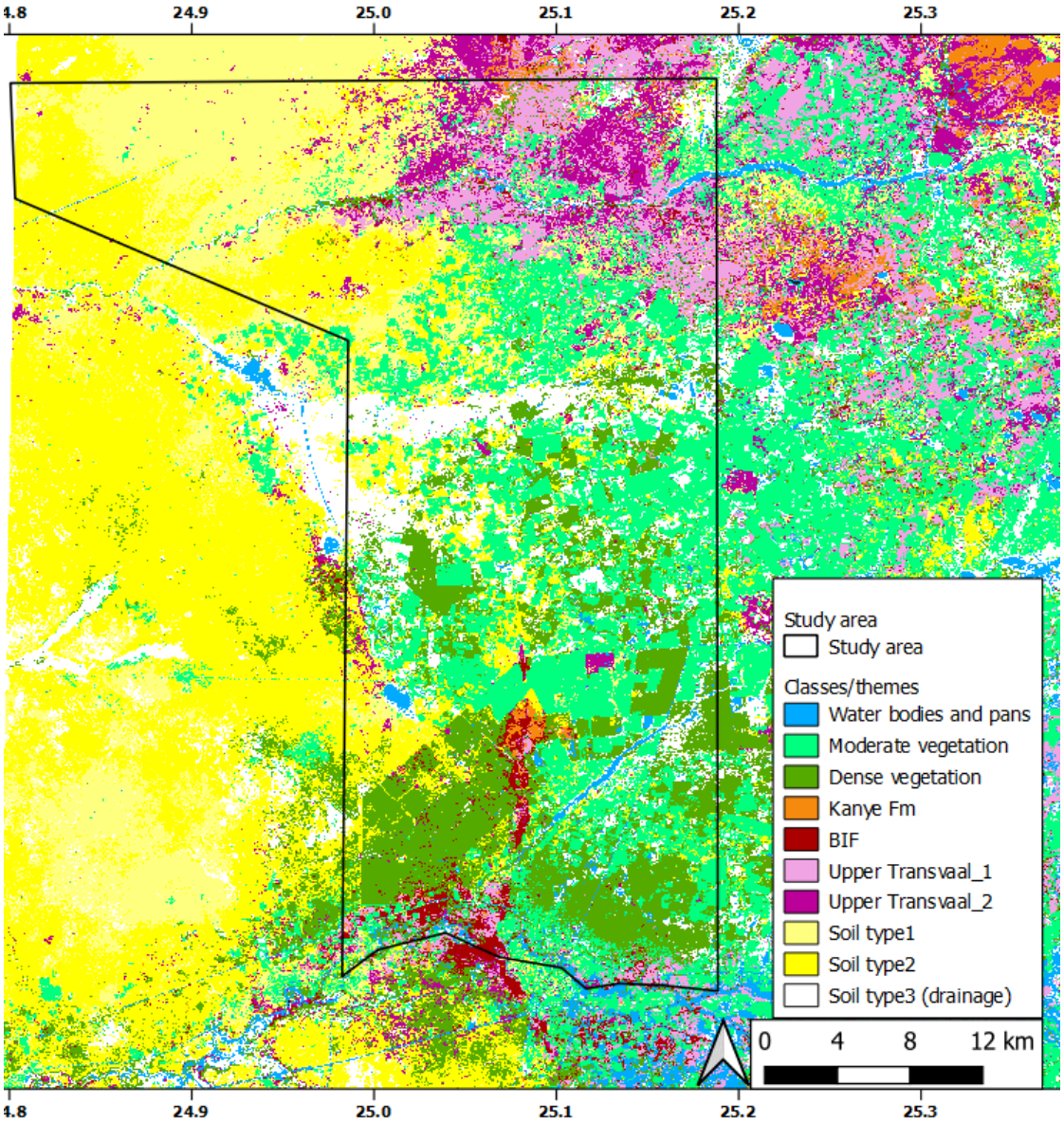


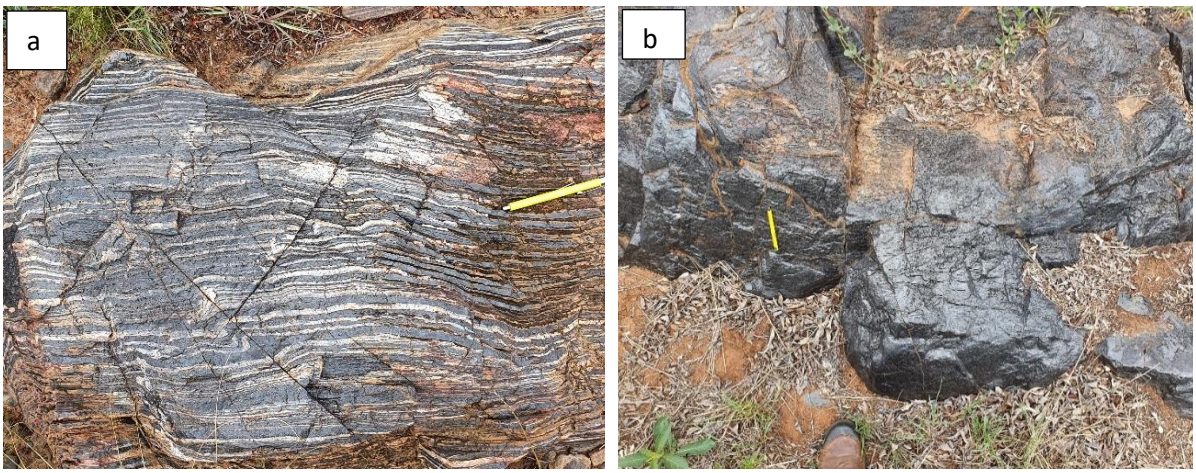
Figure 14. Thematic map generated through supervised classification from Landsat 8 band 1-7 multispectral data, using partly ground-truthed ROIs.

The northern portion of the BIF on the thematic map shows a patch of “Kanye Fm”, which is known to contain volcanic rocks. If that classification is not erroneous, the signature that may be from the volcanic assemblage of the greenstone belt rather than the Kanye Formation rocks themselves. If this interpretation is correct, the remote sensing data was able to map a small portion of the greenstone belt other than the BIF. However, no mapping of the greenstone belt was possible beyond its already known extents. This is certainly due to the extensive soil cover which masks spectral reflectance of underlying rocks, even more so in areas of thicker sand cover. The Landsat-8 bands are 30 m resolution so the accuracy for the mapped lithologies is lower than that of the orthophotos.

4.3.2 Field mapping

BIF is the most common rock outcrop encountered during field mapping. Two main varieties of BIF were noted; one with conspicuous banding with alternating white silica-rich bands and dark iron oxide-rich bands (Figure 15a), and another with visibly less silica content and more obscure banding (bordering on being massive in textural appearance, Figure 15b). The iron oxide occurs mainly in the form of hematite, although the BIFs are magnetite-bearing in some places. No spatial, structural or stratigraphic relations were determined between the two BIFs.

Other rock units included a very fine-grained, thinly banded grey rock with banding defined mainly by quartz ribbons (Figure 15c), and a relatively less competent and strongly foliated to schistose rock with green tinge, possibly due to chloritic and epidote alteration (Figure 15d). The former is most likely a metagreywacke while the latter unit seems to be similar to schistose metabasalts mapped and described by Carney et al (1994) in the Molopo riverbed, which they mentioned as being largely composed of actinolite and chlorite.



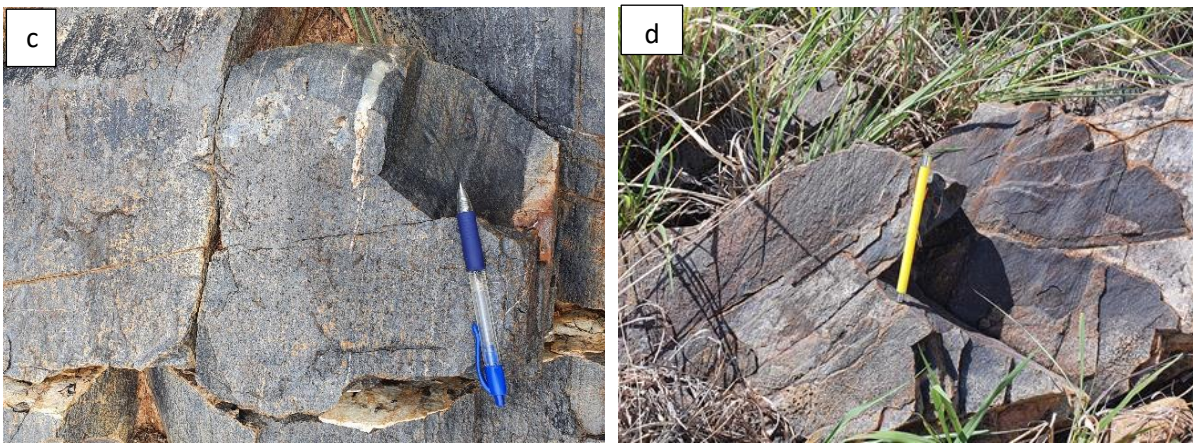


Figure 15. Different rocks units that were encountered during field mapping. (a): thinly banded BIF with conspicuous alternation of silica-rich white bands and iron oxide-rich dark bands. (b): iron oxide dominated BIF with a massive textural appearance. (c): greyish-green greenstone rock (possibly metagreywacke) with a gneissic texture formed by thin, quartz ribbons. (d): highly foliated to schistose rock with epidote and chlorite alteration (hematite and limonite alteration visible along fractures and foliation planes).

The outcropping rocks typically strike northward and dip steeply (greater than 70 degrees on average) toward the west. They are all well-foliated but also exhibit both ductile and brittle structural features, suggesting that the style of deformation evolved as it progressed, and/or several deformation events took place. Figure 16a to d depict some of the structural features observed in the rocks.

In Figure 16a, the BIF contains a tight fold with an interlimb angle of less than 30°. Within the core of that fold are less commonly observed folds whose axial traces are discordant to those of the inclosing fold, suggesting that the two folds formed during separate events; that the enclosed fold must be older and, the orientations were different for the principal stress fields which were responsible for the folding events. Parasitic folds are visible in Figure 16b, indicating that flexural slip has occurred during folding.

A zone of shearing (outlined by white lines), which is parallel to the fold axes, displaces the folded BIF. It is therefore relatively younger than folding (although it may well be contemporaneous with and developed during the progressive ductile deformation). The shear may well serve to indicate strain partitioning. The red ovals in Figure 16b outline zones of brecciation which post-date folding within the BIF, suggesting that either deformation evolved from ductile to brittle regime, or that a later event was responsible for brittle deformation.

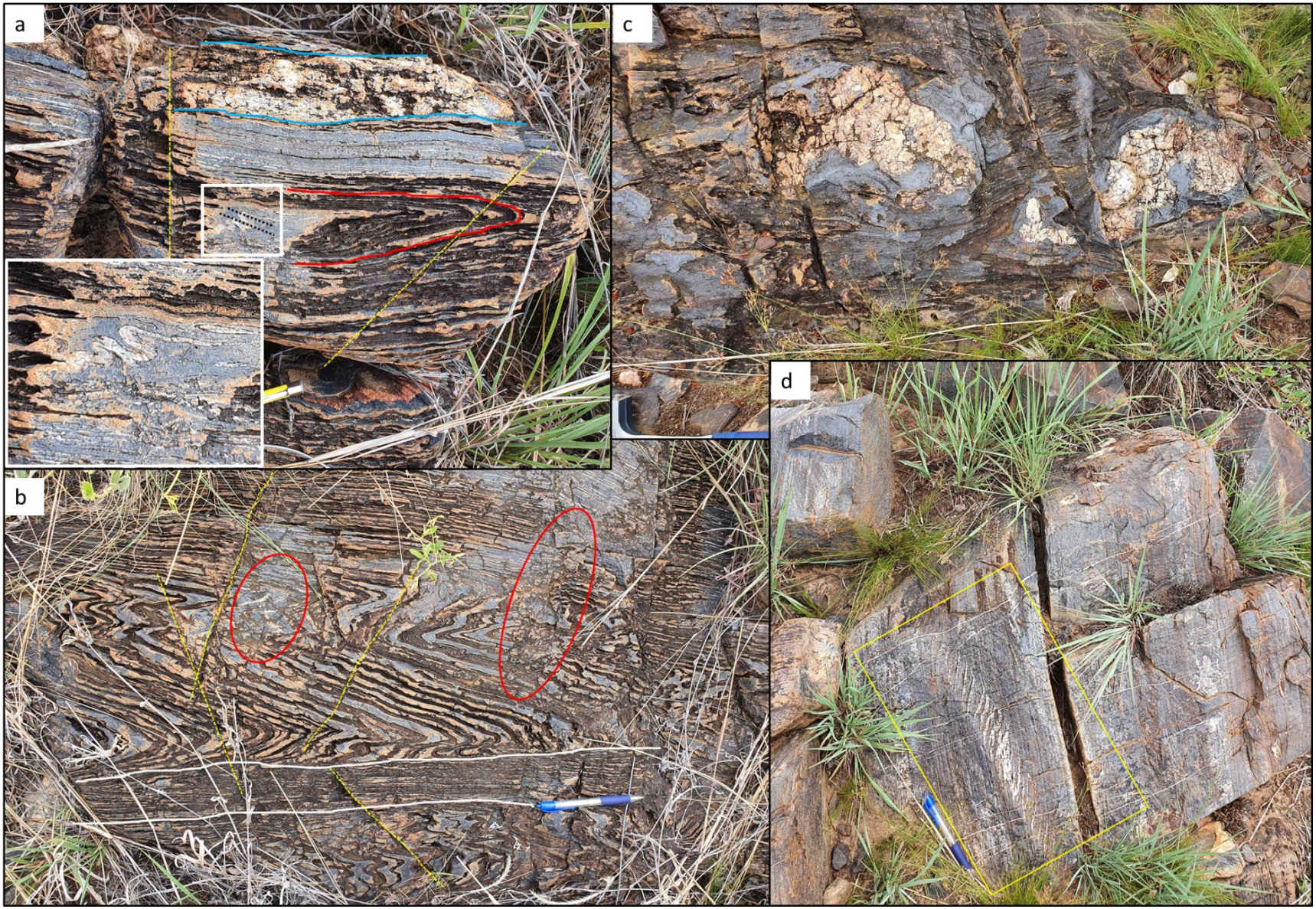

a
b
c
d

Figure 16. Photographs displaying some of the structural features that were observed during field mapping. (A): BIF showing different folding events (red line marking a fold closure of which at its core occurs discordant folds, whose axial traces are marked by black dotted lines – these intrafolial folds must have formed first). Blue lines demarcate a quartz vein while dotted yellow lines mark joints which are probably conjugate sets and have displacement along them. (B): folded BIF with a zone of shearing (white lines), zones of brecciation (within the red ovals) and joints with displacement (dotted yellow lines), that post-date the rest of the structures. (C): boudinaged quartz veining within the BIF. Boudin rims and pressure-shadows have strong iron alteration. (D) metagreywacke with en-echelon tension gashes (within yellow box) whose tips suggest that they opened parallel to the main foliation. These are cross-cut by later perpendicular quartz veins.

It is nonetheless clear in Figure 16c that while ductile deformation lasted, it was accompanied by quartz veining and formation of asymmetrical boudins. Strong hematite alteration is present in the pressure-shadows and rims of the boudins. Vein formation and alteration (which both demonstrate hydrothermal fluid percolation) were however, not observed to be widespread during the mapping exercise. Stress field rotation during deformation is indicated both by the boudin asymmetry as well as the en-echelon tension gashes in the metagreywacke in Figure 16d. The tension gashes are cross-cut by thin quartz veins that are oblique to foliation. It is possible that these are related to the displacement joints marked in yellow in Figure 16a and b, which evidently post-date most structures and are likely to be part of a conjugate set.

A geological map was created in Quantum GIS using field mapping data described above and high-resolution Bing imagery (Figure 17a to d). Areas of negative relief within the outcrops in Figure 17a are largely parallel to the trending direction of those outcrops. They are either underlain by lithologies interbedded with the BIFs, that are prone to weathering or underlain by zones of faulting/shearing. As noted above, flexural slip seems to have accompanied folding. Shear zones parallel to the greenstone have been postulated occasionally noted at the Kalgold and Blue Dot deposits (Anhausser, 1991).

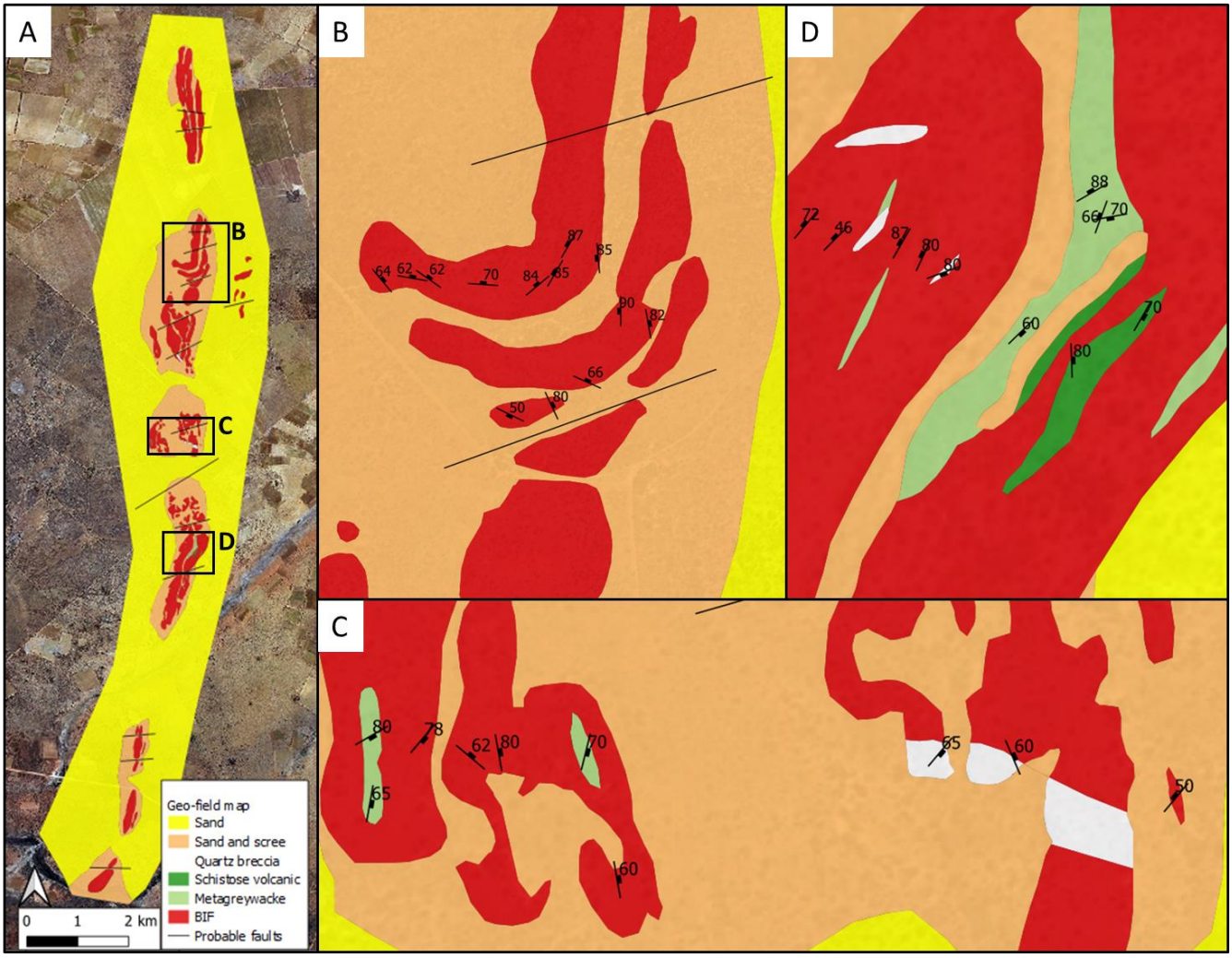


Figure 17. Geological maps of the southern part of the study area, created from field mapping and satellite imagery. (a): overview map showing various lithologies and probable faults shown in black lines. (b): synformal fold within the BIF. (c): predominantly east-dipping part of the greenstone belt. A ~20 m wide of quartz brecciation is present. (d): area with an overall antiformal structure where numerous greenstone lithologies are present.

4.4 Geochemical data and analysis

Geochemical data that is available for the study has been derived and collated from filings of exploration companies which collected the data during their active exploration periods within the study area. No additional geochemical data was collected during the current study. The historical data used for the study is that of sediment samples and down-hole drilling data. The purpose of evaluating the available geochemical data is fourfold.

a) To check for the occurrence of gold-in-soil anomalies and for presence of gold within the drill intersections

b) If gold anomalies and/or intersections are present, to investigate whether they are associated with any pathfinder elements.
c) To investigate whether there are any discernible litho-geochemical trends by determining if the geochemistry of the soil/Kalahari cover can be correlated with the underlying geology, or if there are any pathfinder metal/element associations relating to the down-hole geology, in particular the BIF known to host gold mineralisation.
d) To compare and contrast recovery results (for gold and other elements) from soil samples and drill samples.

4.4.1 Geochemistry from soil samples

The soil samples whose geochemical data is available for the study area were collected in two separate sampling programmes (referred to here as "Soil sampling" 1 and 2, Figure 18). For both sampling programmes, the samples were collected at 50 m spacing, over areas of different Kalahari cover thicknesses. For the sampling programme "Soil sampling 1", the samples lines were oriented east-west and spaced at 200 m. The sampling targeted the area where the BIF outcropped and therefore the samples were derived from where the soil is thin and/or residual (samples there occur largely within the 10 m isopach). The soil samples were screened to a size fraction of less than 53 microns and processed through aqua regia digest, followed by graphite furnace atomic absorption spectrometry (GFAAS) finish. Available analytical results are for gold (in ppb) as well as copper and nickel (in ppm).

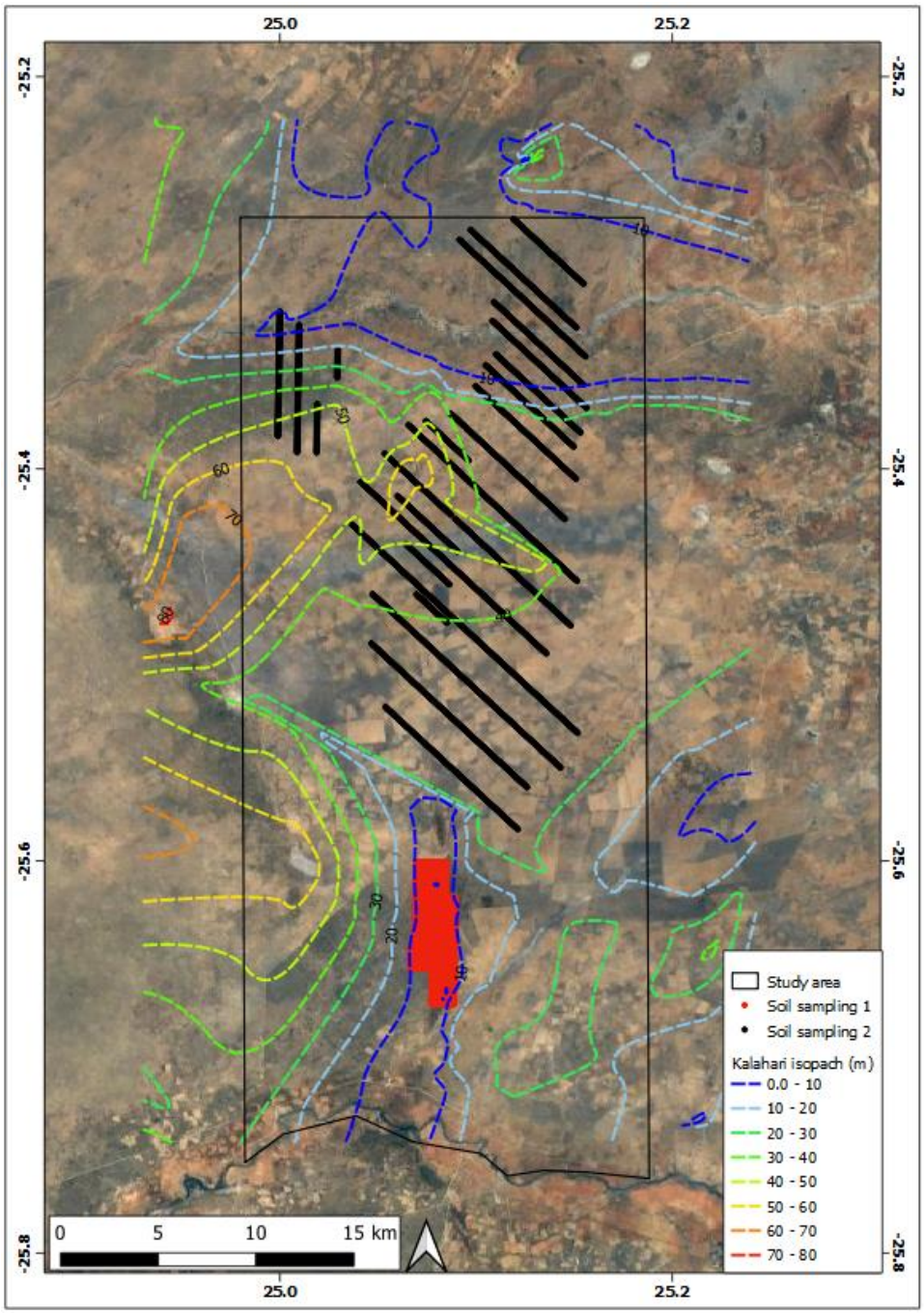


Figure 18. Locations of historical soil samples with assay results within the study area. “Soil sampling 1” samples are depicted by the red sample grid and were collected in the southern portion of the study area where the BIFs are outcropping. “Soil sampling 2” samples are depicted as black sample lines were derived from outside of the know BIF outcrops. Kalahari thickness isopachs are shown to give an idea as to whether the samples are residual or transported.

Assay results for “Soil Sampling 1” are depicted in Figure 19, where they are overlain on satellite imagery where the dark rusty colour coincides with the BIF outcrop. Gold results, in ppb, are shown as polygons, shaded in colours that warm with increasing grade.

Copper and nickel results, both in ppm, are shown as contour lines and transparent polygons respectively. Of the 1511 samples analysed for gold, over 1400 returned results of less than 7 ppb, while the most gold-anomalous sample peaked at 63 ppb. Whereas most samples derived directly over the BIF returned negligible gold results, with only one gold-in-soil anomaly located directly over the BIF. Most of the gold-in-soil anomalies are narrow, with only two occurring in the south of the area that were picked up by more than two consecutive samples on a line (equating to at least 150 m width, at 50 m sample spacing).

Most of the gold-in-soil anomalies were also limited in strike length, with only a few getting picked in more than one sample line (with the lines spaced at 200 m). Two such anomalies are outlined by red rectangles in the southern part of the sample grid, where the southernmost anomaly had a strike length of more than 600 m and a gold peak of 40 ppb. It is difficult to judge the significance of these anomalies. Although the Kalgold mine has a maximum Kalahari thickness of 50 m, the soil anomaly footprint is likely to have been much larger.

Copper and nickel contents of the samples are much higher than gold and their anomaly footprints much more extensive. Nickel contents are comparatively higher than copper, peaking at 165 ppm as opposed to 59 ppm for copper. These two base metals do overlap with each other spatially, but their anomalies only coexist occasionally, however, copper seems to be more widespread while nickel seems to have a negative association with the BIF (Figure 19). A correlation matrix is shown in Table 1 for gold, copper and nickel for the “Soil sampling 1” programme. Correlation coefficients of nickel and copper to gold are low, whereas nickel and copper correlate relatively better with each other.

Table 1. Correlation matrix of Au, Cu and Ni for the “Soil sampling 1” programme.

	Au ppb	Ni ppm	Cu ppm
Au ppb	1		
Ni ppm	0.107	1	
Cu ppm	0.201	0.585	1

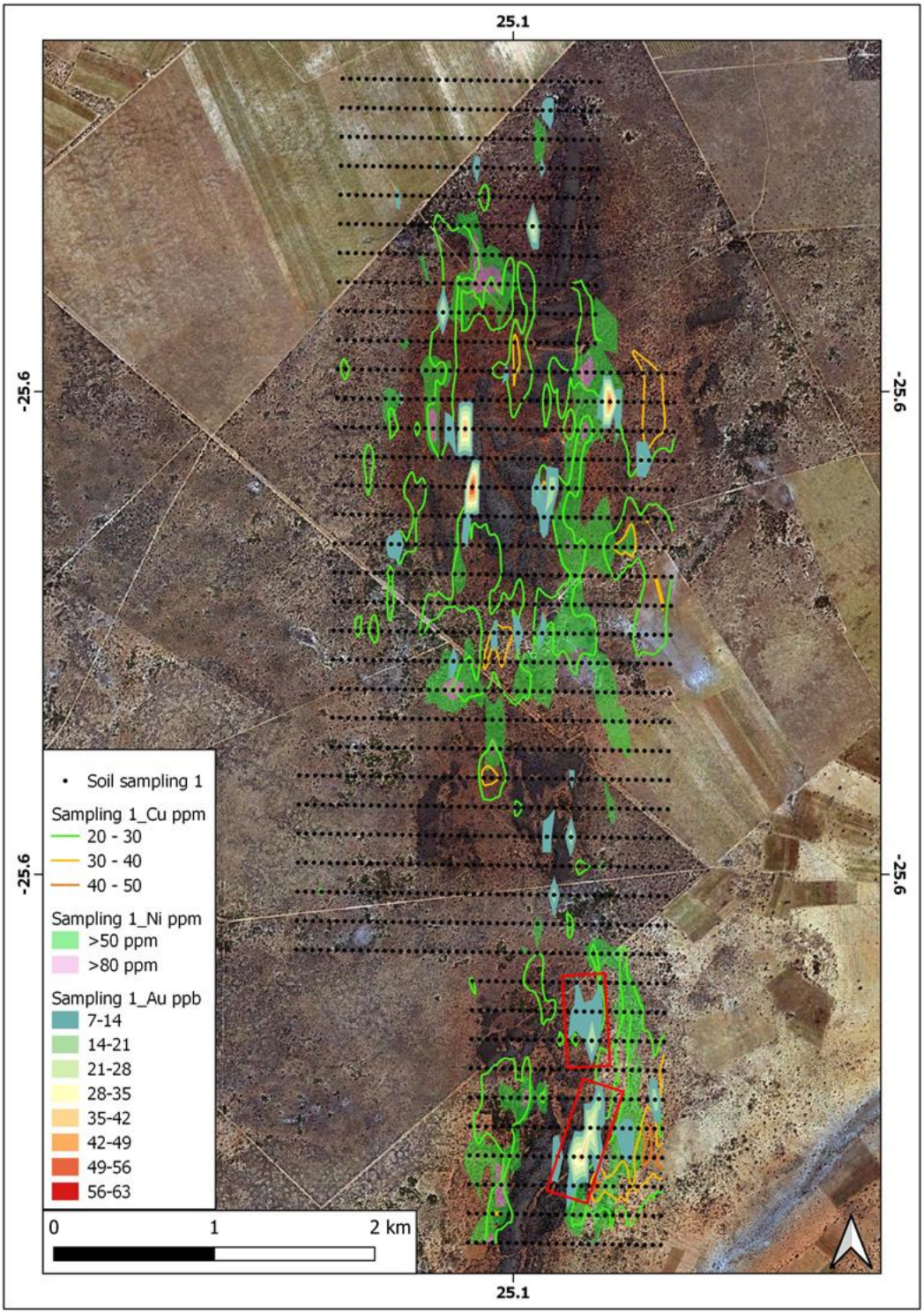


Figure 19. Soil sample results for the "Soil sampling 1" programme are overlain on a Bing satellite image, whose parts with a dark rusty appearance coincide exposed BIF. Soil sample locations are shown as black dots. Most samples returned less than 7 ppb gold while the most anomalous picked at 63 ppb. Copper results are shown as contour lines while nickel results are shown as shaded polygons. Peak results for Ni and Cu (not shown) are 155 ppm and 59 ppm respectively. Most gold-in-soil anomalies are located within or close to the BIF whereas the highest Ni and Cu values are displaced from it. Potentially significant gold anomalies are outlined with red rectangles.

Over 14,000 soil samples were collected during the “Soil sampling 2” programme (Figure 18), by Discovery Metals Limited. Geochemical results were only available for 3,750 samples. The samples were spaced at 50 m and the sample line spacing ranged from 400-2000 m. As opposed to the southern sampling grid “Soil sampling 1”, these samples were derived from areas where rock outcrops are absent and the Kalahari cover thickness is more variable, reaching 60 m in places. Some of the thick Kalahari sediments in those areas include unconsolidated sand, unconsolidated gravels, calcretes and silcretes, as observed from available drill materials and geological logs. The soil samples were collected at a size fraction of 0-180 microns and prepared for analyses by partial acid digest. Low detection analyses were performed for the following minerals in ppb: Au, Ag, As, Bi, Cd, Co, La, Mo, Pd, Pt, Sb, Sn, Th, U, and W; while the elements Cu, Ni, Pb, Sc and Zn were reported in ppm.

A correlation matrix is displayed in Table 2 for selected elements which are generally known to be good pathfinders for gold. The metal contents are low for gold and the selected elements from the sample programme. As a result, the correlation coefficients are also low (perhaps due to low recoveries rather than lack of correlations). Figure 20 spatially depicts the assay results for silver, copper and nickel so as to visually compare them to gold results (as they seemed to have a weak correlation). Copper and nickel were also chosen because they were analysed in in the Soil sampling 1 programme.

Table 2. "Soil sampling 2" correlation matrix for selected potential gold pathfinder elements.

	Au_ppb	Ag_ppb	As_ppb	Bi_ppb	Cu_ppm	Ni_ppm	Pb_ppm	Sb_ppb	Zn_ppm
Au_ppb	1								
Ag_ppb	0.0900	1							
As_ppb	0.0782	0.2438	1						
Bi_ppb	-0.0059	0.0231	0.3898	1					
Cu_ppm	0.0885	0.7548	0.5116	0.2264	1				
Ni_ppm	0.0799	0.4158	0.6764	0.4950	0.6902	1			
Pb_ppm	-0.0532	-0.3012	0.2301	0.6078	-0.1224	0.2536	1		
Sb_ppb	0.0128	0.2121	0.6294	0.5564	0.4997	0.6754	0.4616	1	
Zn_ppm	0.0046	-0.1529	0.5175	0.5612	0.1714	0.5902	0.6563	0.6074	1

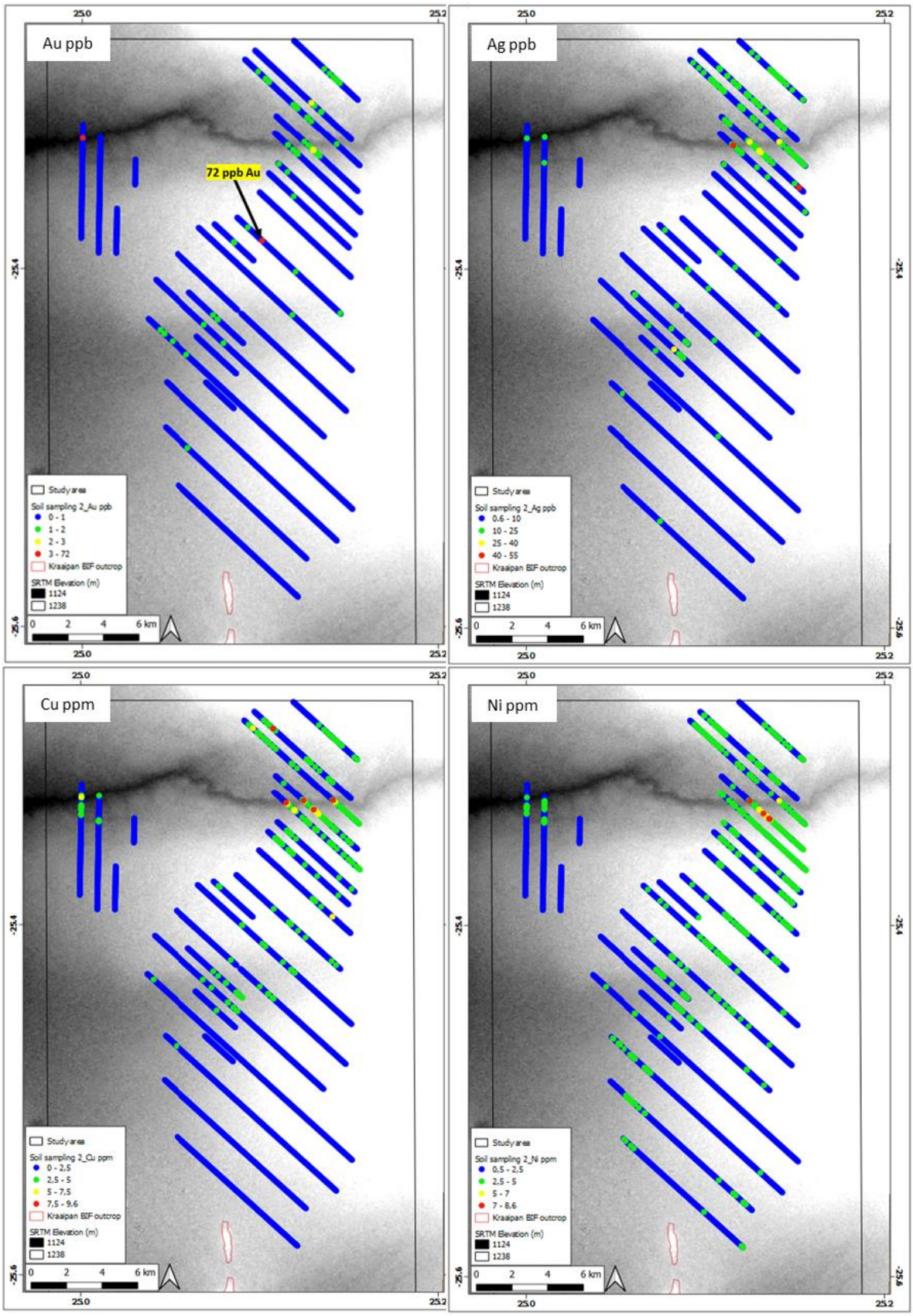


Figure 20. Location maps of "Soil sampling 2" programme soil samples overlain on an SRTM image. Assay results for gold (ppb), silver (ppb), copper (ppm) and nickel (ppm) are displayed from top-left to bottom-right. For all of the metals, the highest assay results occur in the

northern part of the study area where a drainage system is present. However, that area is also known to be overlain by relatively thin soil cover. No unambiguous correlations exist between gold and the rest of the metals occur within and outside of this area.

The gold-in-soil results are generally low and range from 0 to 4.7 ppb, with a single outlier of 72 ppb. Ag, Ni and Cu content range from 0.6-55 ppb, 0.5-8.6 ppm and 0.2-9.6 ppm respectively. Au, Ag, Cu and Ni counts range from the least to most widespread in that order, and all of the metal counts are higher in the northern part of the study area. This seemingly anomalous area coincides with a low-lying drainage system, where the highest assay results are closet to the riverbed, as seen from the SRTM backdrop image (Figure 20). The area is also overlain by relatively thin soil cover (less than 10 m, some of which could be residual). The gold result of 72 ppb, which is an outlier for the assay results, cannot be explained by means of pathfinder element associations and therefore it's significance cannot be confirmed. Analytical discrepancies cannot be ruled out. The fact that the samples were collected at a size fraction of -180 microns could be suggestive of a nugget effect for this result.

For the "Soil sampling 1" programme, the samples were collected at size fraction of -53 microns and the gold, nickel and copper results ranged from 0-63 ppb, 11-155 ppm and 2-59 ppm respectively. These are much higher than the results for "Soil sampling 2" programme. Explanations for the disparity in metal content for the two sampling programmes could be one of a combination of the following factors: Kalahari cover thickness, soil sampling technique and analytical methods. The samples with the highest metal content were derived from areas of thinner Kalahari cover for both sampling programmes (although drainage is likely to have had an effect on "Soil sampling 2" results).

4.4.2 Historical Drilling results

This section focusses on drilling activities carried out with the purpose of intersecting gold mineralisation within the study area. Three exploration drill programmes were carried out historically. The drill programmes targeted geophysical anomalies; surface geochemical results; and previous drilling results.

Reunion Mining Botswana conducted a percussion drilling programme consisting of 78 drill holes totalling 3791 m (Figure 21). The programme was designed to follow up on geochemical

anomalies identified from their “Soil sampling 1” programme. Drilling was conducted along drill-fences roughly perpendicular to the local strike of the geology. The best drill intersections are summarised in Table 3. Reunion concluded that the gold mineralisation within the BIFs was of limited width and down-dip extent, with the low probability of near-surface economic gold deposits being present.

Table 3. Summary of Reunion Mining’s historical gold mineralisation intersections within the Kraaipan greenstone belt of Botswana.

Hole ID	Au grade	Specified Au grade
KRP037	13m @ 1.7 g/t	3m @ 5.1 g/t
KRP052	21m @ 1.0 g/t	5m @ 2.3 g/t
KRP077	9m @ 1.1 g/t	4m @ 2.3 g/t
KRP074	42m @ 0.6 g/t	21m @ 1.0 g/t

Laconia Resources conducted two drill programmes comprising 32 reverse-circulation drill holes (2,941 m) and four diamond core drill holes for 715.4 m (Figure 21). They targeted both gold mineralisation within the Kraaipan Group rocks and potential metal sulphides within intrusive mafic-ultramafic bodies of the Molopo Farms Ultramafic Complex which intrudes into the northern part of the study area. Magnetic data was used to target possible BIF for the gold, whereas pre-existing VTEM airborne electromagnetic survey and ‘Moving Loop’ ground electromagnetic survey (MLEM) datasets were used to identify conductive anomalies for possible Ni-Cu-(Au) sulphides. Where possible, geochemical soil results from “Soil sampling 1 and 2” geochemical sample grids were utilised to support the drill targets.

Drilling results did not return any significant gold or base metal assay results. The only boreholes with positive results came from the holes that targeted the historical Reunion boreholes which intersected encouraging gold results (Tables 3 and 4, Figure 21).

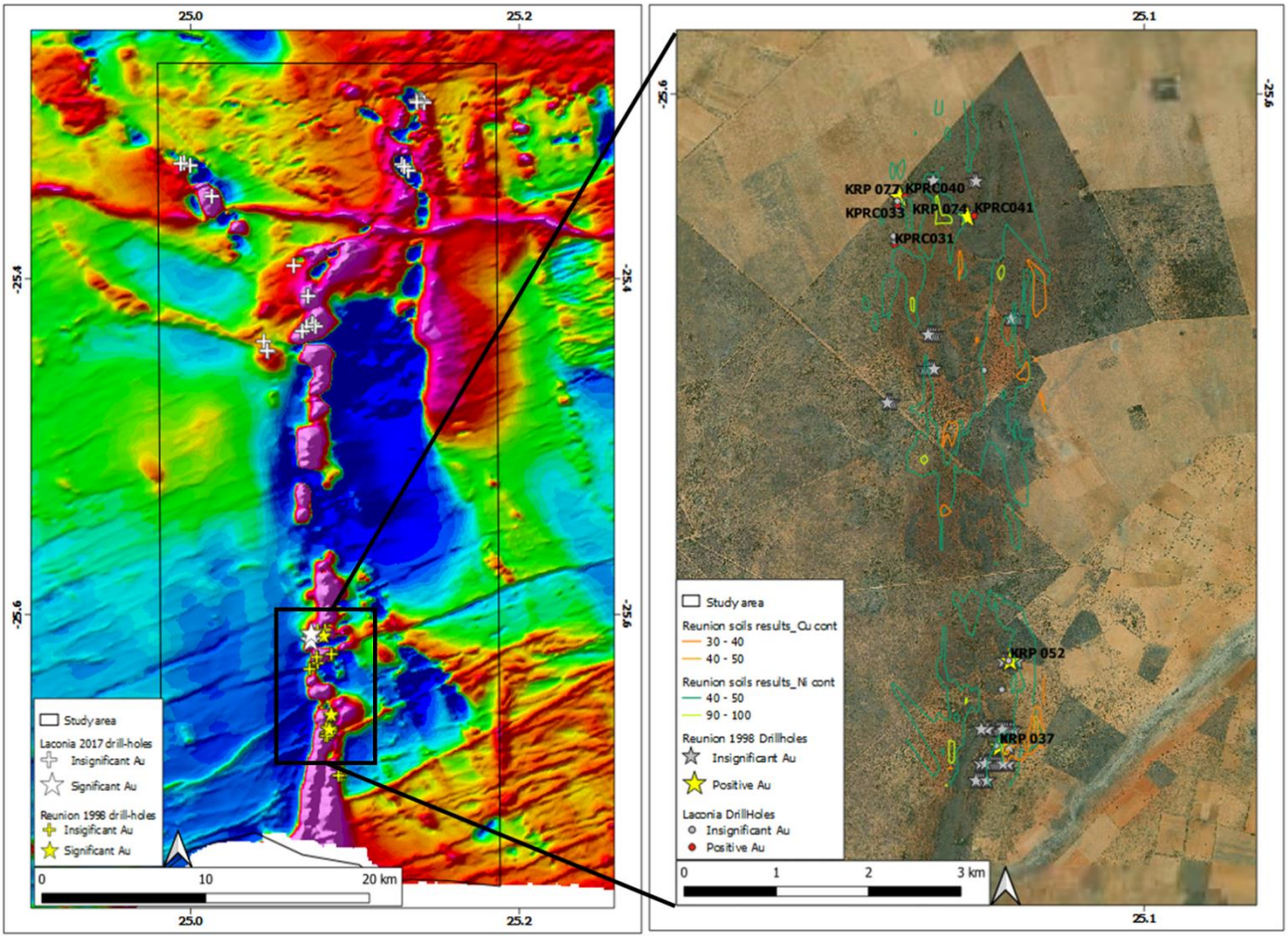


Figure 21. Locations of historical boreholes within the Kraaipan Greenstone Belt of Botswana. Left: boreholes overlain on a reduced-to-pole total magnetic intensity image. The drilling programmes were carried out by different companies. Right: enlarged area where all drill-holes with gold intersections are located. They are all located within and around where banded iron formations are outcropping.

Table 4. Summary of Laconia Resources' mineral intercepts within the Kraaipan Greenstone Belt of Botswana.

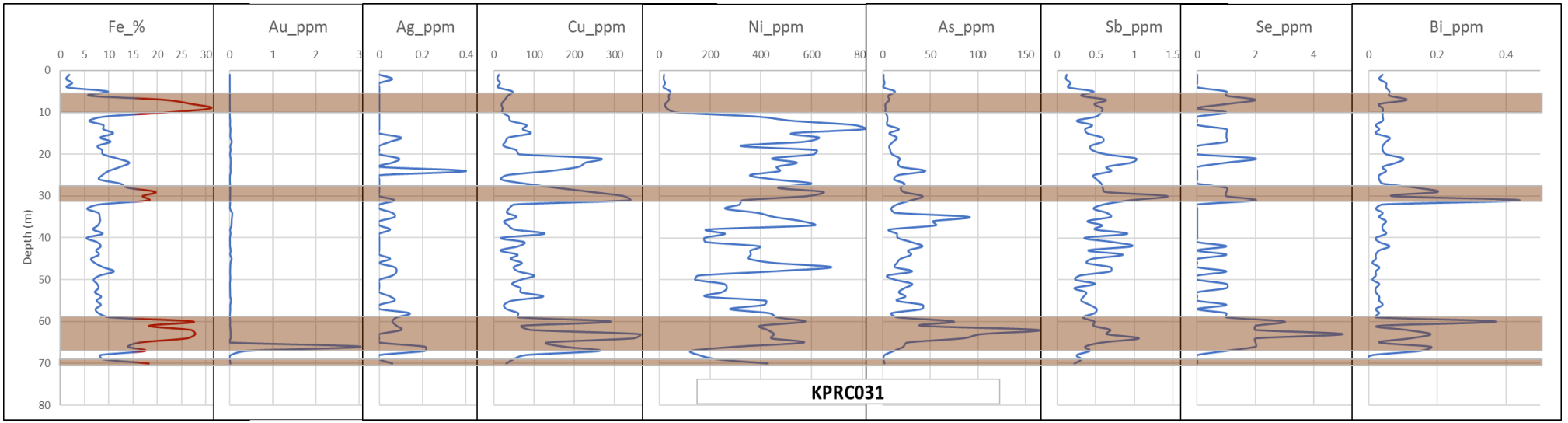
Hole ID	Au grade	Mineralised depth	Drilling rationale
KPRC031	2m @ 1.72 g/t	65-67 m	Follow up on historical geochemical anomaly
KPRC033	5m @ 0.14 g/t	43-48 m	Follow-up on KRP077 historical results.
KPRC040	1m @ 2.25g/t 2m @ 0.84g/t 1m @ 0.55g/t	48-49 m 63-65 m 71-72 m	Follow-up on KRP077 historical results.
KPRC041	2m @ 0.67 g/t 1m @ 0.57 g/t	62-64 m 45-46 m	Follow up on KRP074 historical results.

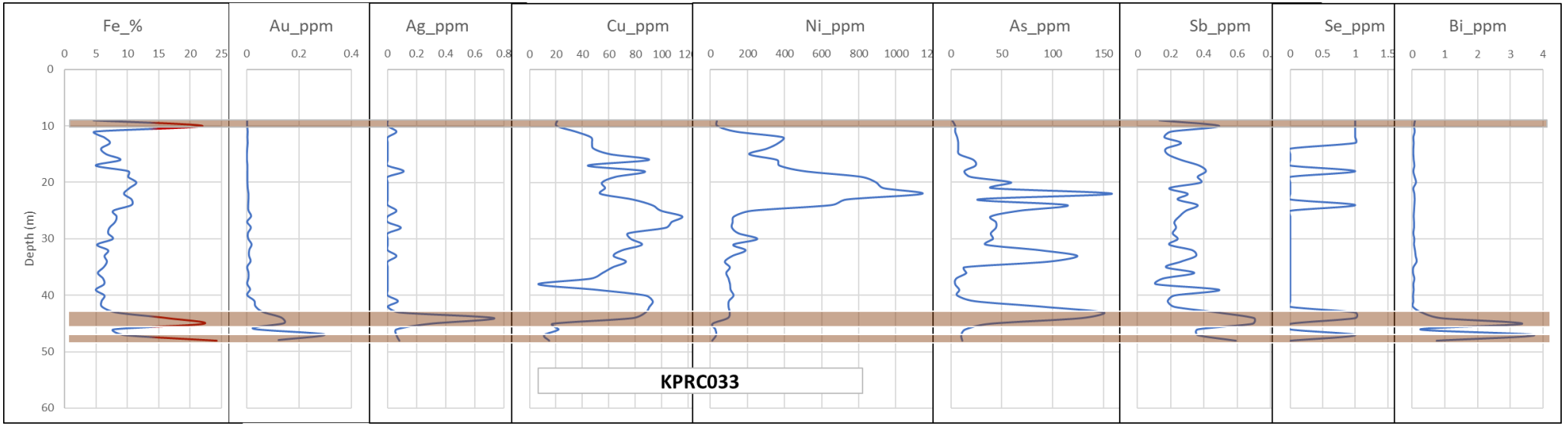
4.4.2.1 Geochemical results from drill samples

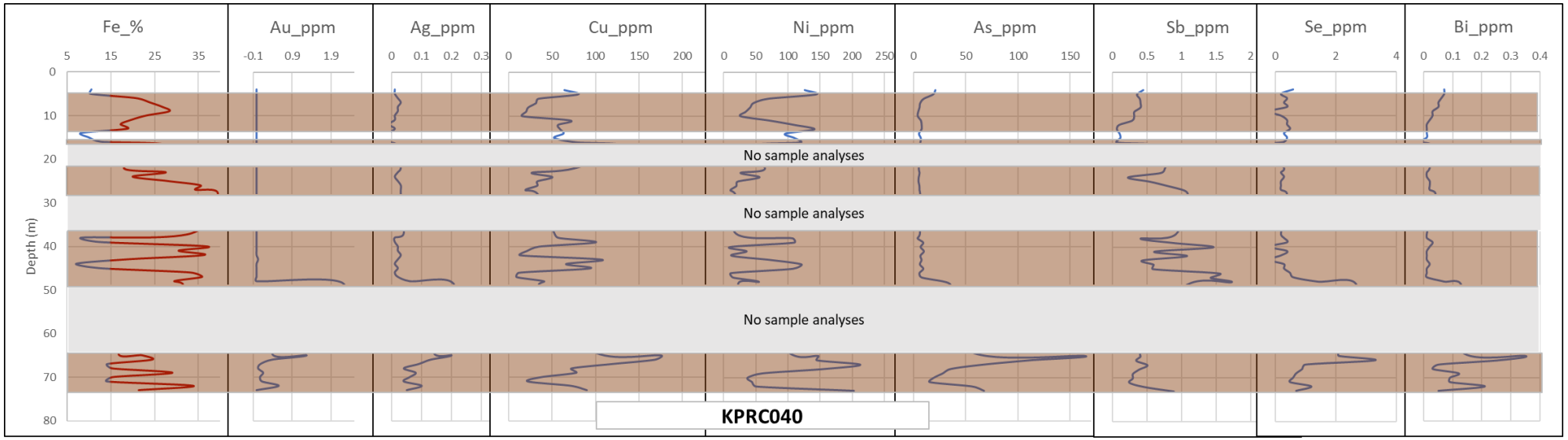
In excess of 240 boreholes have been drilled historically within the study area, which may be incomplete. The majority of which are water boreholes with no recorded geological information. Only 22 boreholes have down-hole geochemical data with no geological logs and no material available for logging. As the gold mineralisation is of particular interest to the study area, attention was only paid to the boreholes which returned positive gold assay results. Four boreholes were chosen (Table 4), with the best gold intersections and accompanying elements, which were used to determine geochemical relationships between the gold and pathfinder elements known for gold deposits.

Down-hole geochemical plots were generated for four boreholes (KPRC031, KPRC033, KPRC040 and KPRC041) depicting iron in percent and gold, silver, copper, nickel, arsenic, antimony, selenium and bismuth in ppm (Figure 22).

BIFs are known to contain 15% or more of iron. Iron contents of the analysed borehole intersections were plotted, and those contents greater that 15% were highlighted for the purpose of indicating the likelihood of those intersections being BIF (Figure 22). No other rock units other than BIF, within the study area are expected to contain similar or higher iron contents, therefore this assumption is considered to be reasonable.


Fe_%
Au_ppm
Ag_ppm
Cu_ppm
Ni_ppm
As_ppm
Sb_ppm
Se_ppm
Bi_ppm
Depth (m)
KPRC031


Fe_%
Au_ppm
Ag_ppm
Cu_ppm
Ni_ppm
As_ppm
Sb_ppm
Se_ppm
Bi_ppm
Depth (m)
KPRC033


Fe_%
Au_ppm
Ag_ppm
Cu_ppm
Ni_ppm
As_ppm
Sb_ppm
Se_ppm
Bi_ppm
Depth (m)
No sample analyses
No sample analyses
No sample analyses
KPRC040

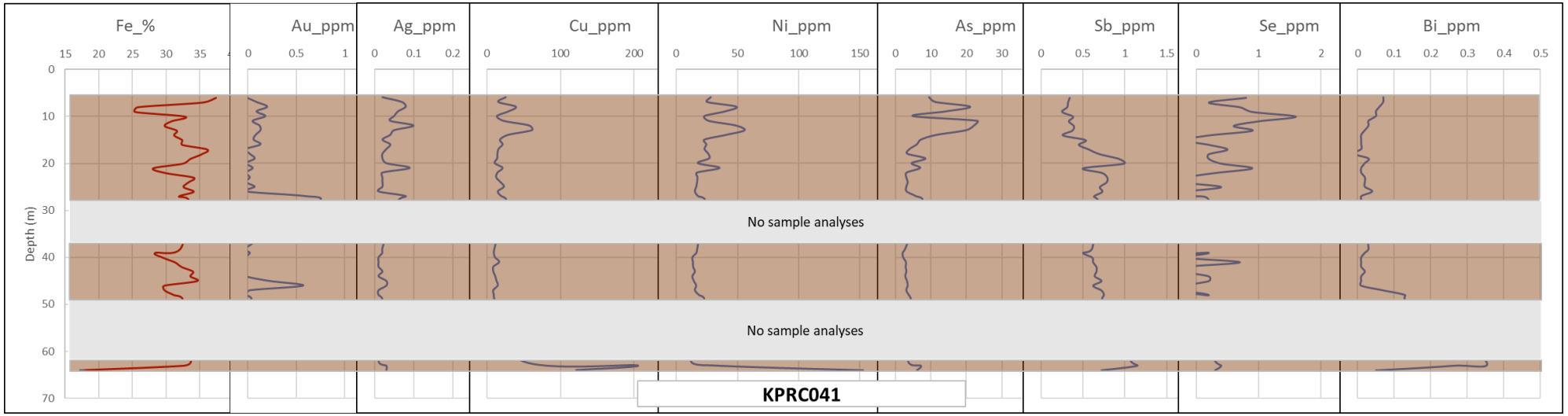

Fe_%
Au_ppm
Ag_ppm
Cu_ppm
Ni_ppm
As_ppm
Sb_ppm
Se_ppm
Bi_ppm
Depth (m)
No sample analyses
No sample analyses
KPRC041

Figure 22. Down-hole geochemical logs of four boreholes (KPRC031, KPRC033, KPRC040 and KPRC041) drilled within the study area. The boreholes contain some of the best gold intersections within the study area. Drill intersections with 15% or more Fe content are inferred to likely be BIF (light-brown bands), on the basis that the BIFs are known to contain iron contents of that range. In all boreholes, gold results are anomalous only within the inferred BIFs. Ag, Cu, Ni, As, Sb, Se and Bi (all in ppm) have been plotted down-hole and they generally correlate well with gold contents.

In all instances, peak gold results occurred within the interpreted BIF intersections. However, gold was not elevated within all of these intersections, nor is it elevated throughout the entire length of any of the supposed BIF. All of the plotted elements have a positive correlation with gold where gold is elevated and are therefore regarded as potentially useful pathfinder elements. Antimony and bismuth in particular are generally low where gold content is low.

5 Discussion

5.1 BIF hosted gold deposits

Archaean gold systems are dominated by orogenic- and Witwatersrand-type gold deposits. The former, which occur in orogenic settings, are generally hosted in greenstone rocks. Gold deposits in these metamorphosed volcano-sedimentary rocks are distributed irregularly, both spatially and in size, and whilst there many gold showings, only 1% can be regarded as deposits (Pearton and Viljoen 2017). One of the subtypes of the orogenic gold deposits is the strata-bound type hosted in BIFs. While many deposits have been classified into this subtype, very few occur in the BIF as the primary host rock (Steadman et al., 2014). One of the exceptions is the > 40-million-ounce gold Homestake Deposit in South Dakota, Steadman and Large (2016).

Other notable BIF-hosted gold deposits include the Randalls Gold District, Yilgran Craton Western Australia; Musselwhite Mine, Superior Province, Canada; Meadowbank, Western Churchill Province; Kalgold Mine (with which the current study is concerned); amongst others. Two gold deposits which occur outside of the Kaapvaal Craton are summarised below and can offer useful direct comparisons with the Kraaipan granite-greenstone terrane setting. They are: Homestake deposit which is BIF-hosted supergiant and the Challenger deposit, which is located in a secondary environment similar to that of the study area.

5.1.1 Homestake Mine

Having produced well over 40 million ounces of gold from 1876 to 2001, the Homestake Mine (located in northern Black Hills of South Dakota USA; Figure 23a) is one of the largest hydrothermal gold deposits in the world (Morelli et al., 2010). The mine is located in the northern end of Black Hills uplift – a tectonic block that has experienced successive uplifts (530 Ma, and 60-65 Ma) and erosion, thereby exposing its Precambrian core as an inlier (Caddey et al., 1991). The Precambrian volcano-sedimentary package which is deemed to be of importance to mineralisation has been subdivided into three formations, which in chronological order are namely, Poorman Formation; Homesake Formation and Ellison Formation (Caddey et al., 1991; Morelli et al., 2010).

All of the mineralisation is hosted within the Homestake Formation (Figure 23b), which comprises metamorphosed iron formations that occur broadly as two endmembers: the iron-carbonate and iron-silicate varieties (siderite-dominant phyllite and grunerite-dominant schist

respectively), both of which are interbedded with ubiquitous thin layers of chert (Caddey et al., 1991; Morelli et al., 2010). The Homestake Formation is underlain by the Poorman Formation (turbidites and schists of tholeiitic protolith) and unconformably overlain by the Ellison Formation (interbeds of quartzitic, pelitic to semipelitic and tuffaceous strata – Caddey et al., 1991). A depositional period of 2,012–1,974 Ma has been evoked for the Homestake Formation, based on age dating of associated igneous/volcanic rocks.

Mineralised strata reached upper greenschist to lower amphibolite facies metamorphism, whereby the Homestake Formation appears to have been relatively intensely deformed compared to the adjoining strata (Caddey et al., 1991). Five deformation events (D1-D5) have been recognised by several workers and are summarised by Morelli et al. (2010) as follows:

- D1: 1,785 to 1,775 Ma northward accretion of the Yavapai island arc resulting in layer-parallel schisosity S1.
- D2: around 1,760 to 1,750 Ma Wyoming-Superior continental collision resulting in upright isoclinal F2 folds accompanied by S2 development and attainment of peak metamorphism.
- D3: formation of S3, mainly by rotation of pre-existing S2 into a subparallel orientation.
- D4: overprinting of D3 structures and refolding of F2 folds into gently-moderately plunging folds (and has thus gone unrecognised by most workers). The deformation event was largely concentrated in the Homestake Formation and is interpreted to have been responsible for all of the gold mineralisation. It progressively evolved from a ductile to brittle regime.
- D5: caused top-to-the-west mm-scale shears and development of steeply dipping S4. This phase marks post-ore brittle deformation.

Orebodies are generally concentrated at the stratigraphic contacts of the Homestake Formation and the adjoining formations. Orezones occur exclusively in the synformal structures (comprised of secondary folds), whereas the interconnecting anticlinal folds and their associated limbs are generally barren (Figure 23c). The synforms are generally more structurally complex than the antiforms (Caddey et al., 1991). Gold mineralisation is in the form of massive sulphide segregations, primarily arsenopyrite and pyrrhotite (and pyrite to a lesser extent). Two types or ores are recognised namely shear and replacement ores. The former occurs within or adjacent to dilated sections of D4 shears, while the latter occurs as

replacements of siderite in zones of permeability (which also developed during D4; Morelli et al., 2010).

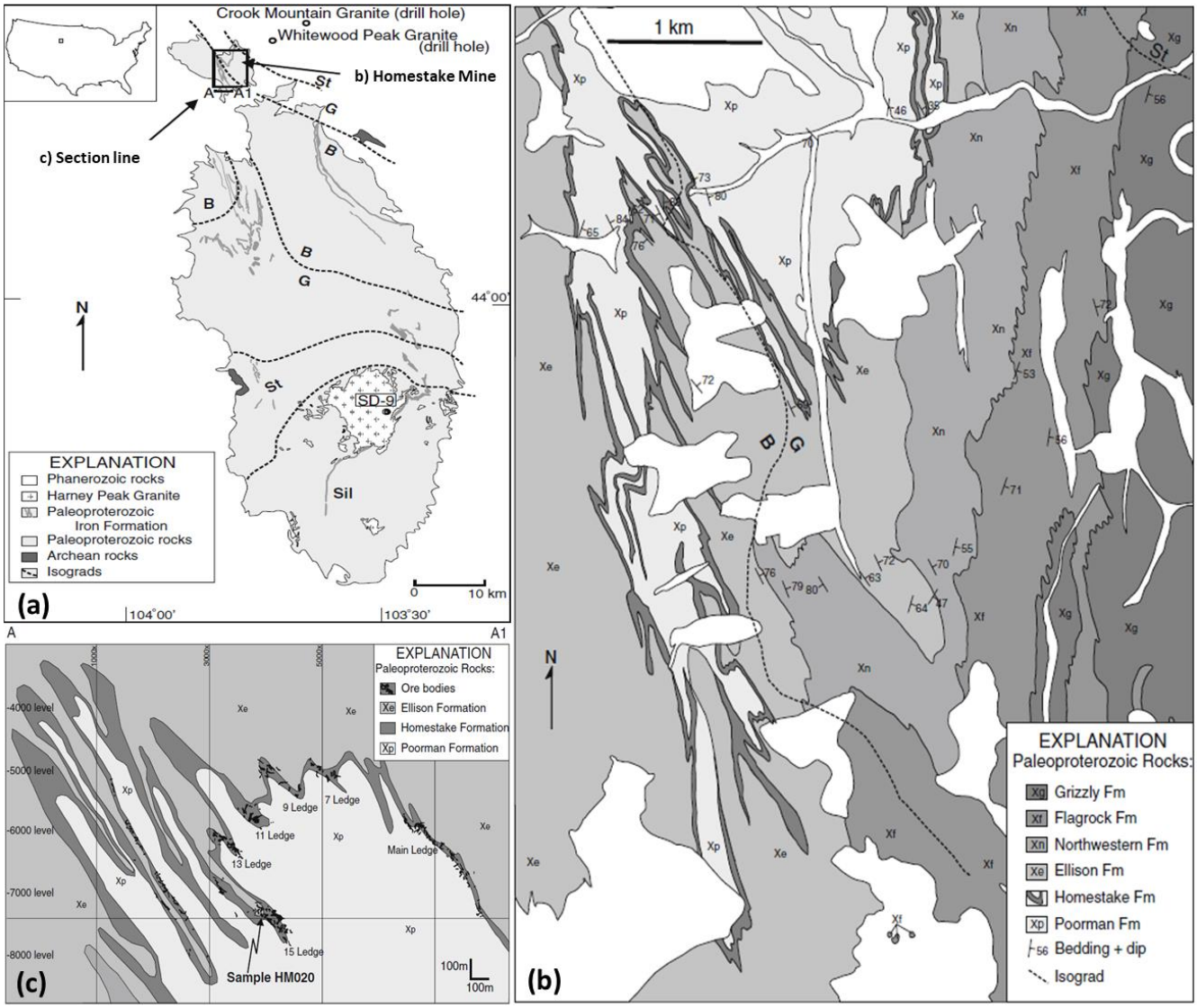


Figure 23. (a) Geology of the Black Hills uplift showing metamorphic isograds for biotite (B), staurolite (St), garnet (G) and sillimanite (Sil). (b) Lithostructural map of the Homestake Mine area. (c) Subsurface geology along a section through Homestake Mine. Orebodies occur as "odd number ledges" in the synformal fold structures. Adapted from Morelli et al. (2010).

Mineralisation post-dates peak metamorphic events as demonstrated by the fact that orebodies are relatively undeformed and exhibit a generally tabular to pipe-like morphology termed "ledges". It is also closely associated with one or more of the following alteration phases: chlorite, biotite, sericite, carbonate and quartz, signifying the role of retrograde hydrothermal alteration as a mineralising event (Morelli et al., 2010).

It is widely accepted that the deposit is of epigenetic origin, whereby auriferous hydrothermal fluids were introduced into the stratigraphy from an external source and trapped by the chemically favourable iron formation (Morelli et al., 2010). In addition to favourable stratigraphy, mineralisation was undoubtably controlled by development of dilatational shears during tectonism as well as hydrothermal activity which post-dates peak metamorphism (Caddey et al., 1991).

5.1.2 Challenger Deposit

The Challenger deposit is located 750 km north-west of Adelaide in Australia (Figure 24). It is hosted with Archaean rocks of the Gawler Craton and specifically the Christie Gneiss, which is a garnet-rich paragneiss with an age of 3070 – 2680 Ma (Williams et al., 2003). The gneiss attained granulite-facies metamorphism during Sleaford Orogeny at 2640-2300 Ma and comprises of the following mineral assemblage: plagioclase, perthitic K-feldspar, quartz, cordierite, garnet and biotite (Williams et al., 2003). There is consensus that gold mineralisation is pre- to syn-orogenic and is associated with silica and arsenopyrite alteration (Lintern, 2015). However, there is some gold which is associated with chlorite, and it is likely to have formed during the retrograde stages (Williams et al., 2003).

The Gawler Craton is characteristically flat-lying and outcrop is sporadic. In many parts of it, including the greater Challenger area, there is a ubiquitous layer of calcrete which may have formed by factors that include: the flat topography, permeable sand cover, and evaporation rates that far exceed precipitation (Williams et al., 2003, Dart, 2009 and Lintern, 2015). These occur as 1-2 m thick horizons just below the surface and is present in various forms namely, nodular, laminated, massive and coatings on sand grains (Lintern, 2015).

Challenger was discovered in 1995 as a direct result of geochemical calcrete sampling and is the first ever deposit to have been discovered in this way. The initial sampling programme was conducted 1.6 x 1.6 km grid spacing and subsequently lead to defining a 4 km^2 5 ppb gold anomaly which peaked at 180 ppb in a sample that was collected directly over the deposit (Williams et a., 2003 and Lintern, 2015). Later calcrete sampling programmes further defined the anomaly, with one sample located directly over the deposit peaking at 2370 ppb (Lintern, 2015). The discovery may have been fortuitus due to the fact that the peak sample was derived directly over the near-surface gold deposit, but the calcrete sampling technique has since

become a phenomenon, with prospects such as Tunkillia and Edolden Tank having been discovered in the same way (Figure 24).

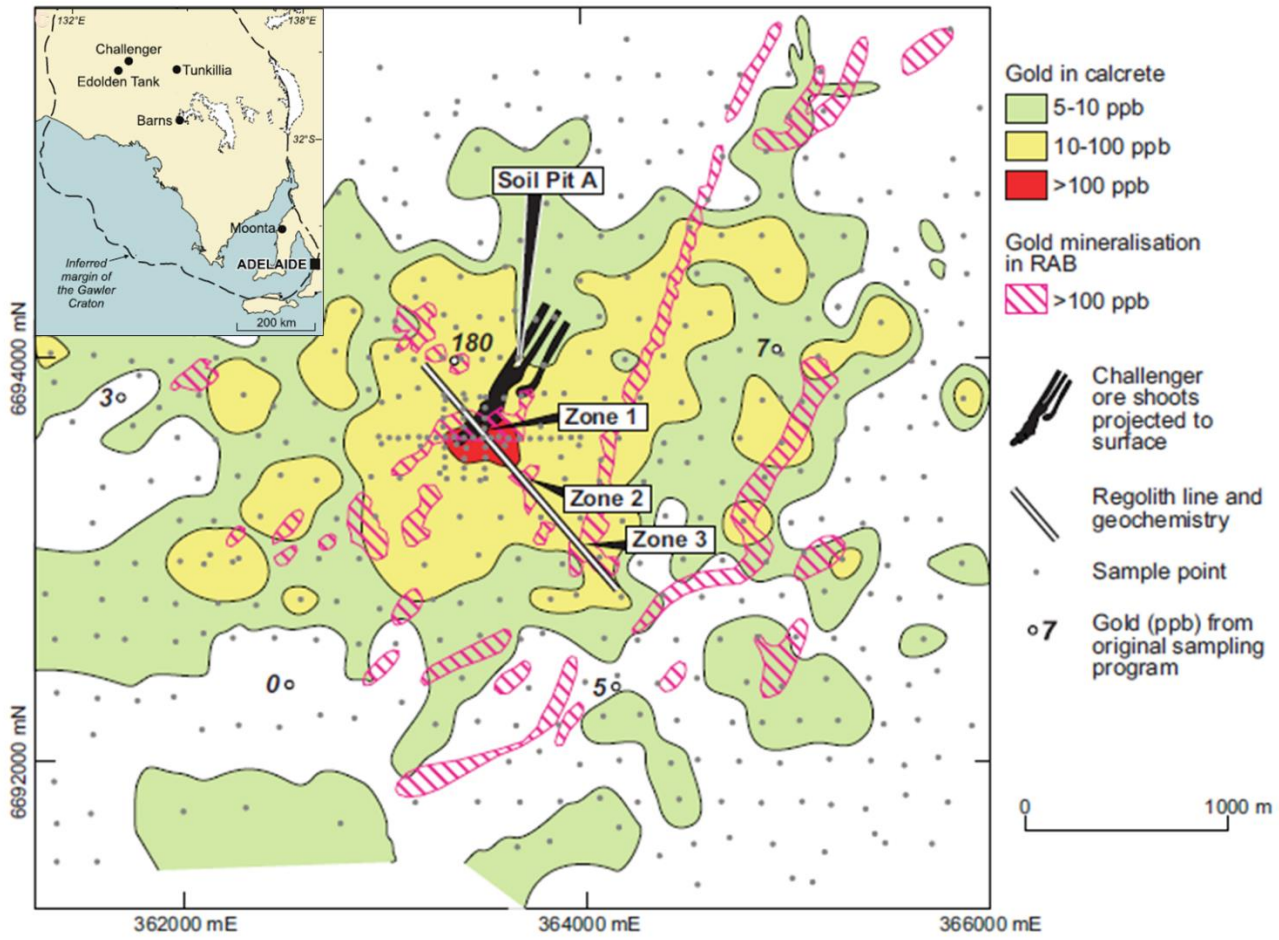


Figure 24. Gold in calcrete anomalism at Challenger. Mineralisation only comes to surface in Zone 1. (Modified from Lintern, 2015)

Figure 25a depicts downhole profiles of gold and calcium contents. These elements generally correlate well, confirming the gold-in-calcrete anomalism. The profile of Pit A does not reveal gold anomalism at surface, even though Pit A is underlain by shoots. That is because the calcium content there increases with depth. Figure 25b and c also show that transported material that underlies can have an effect of masking gold anomalies, as seen in the case of Zone 3. This reinforces the importance of understanding the regolith of an area of interest in order to correctly interpret geochemical results.

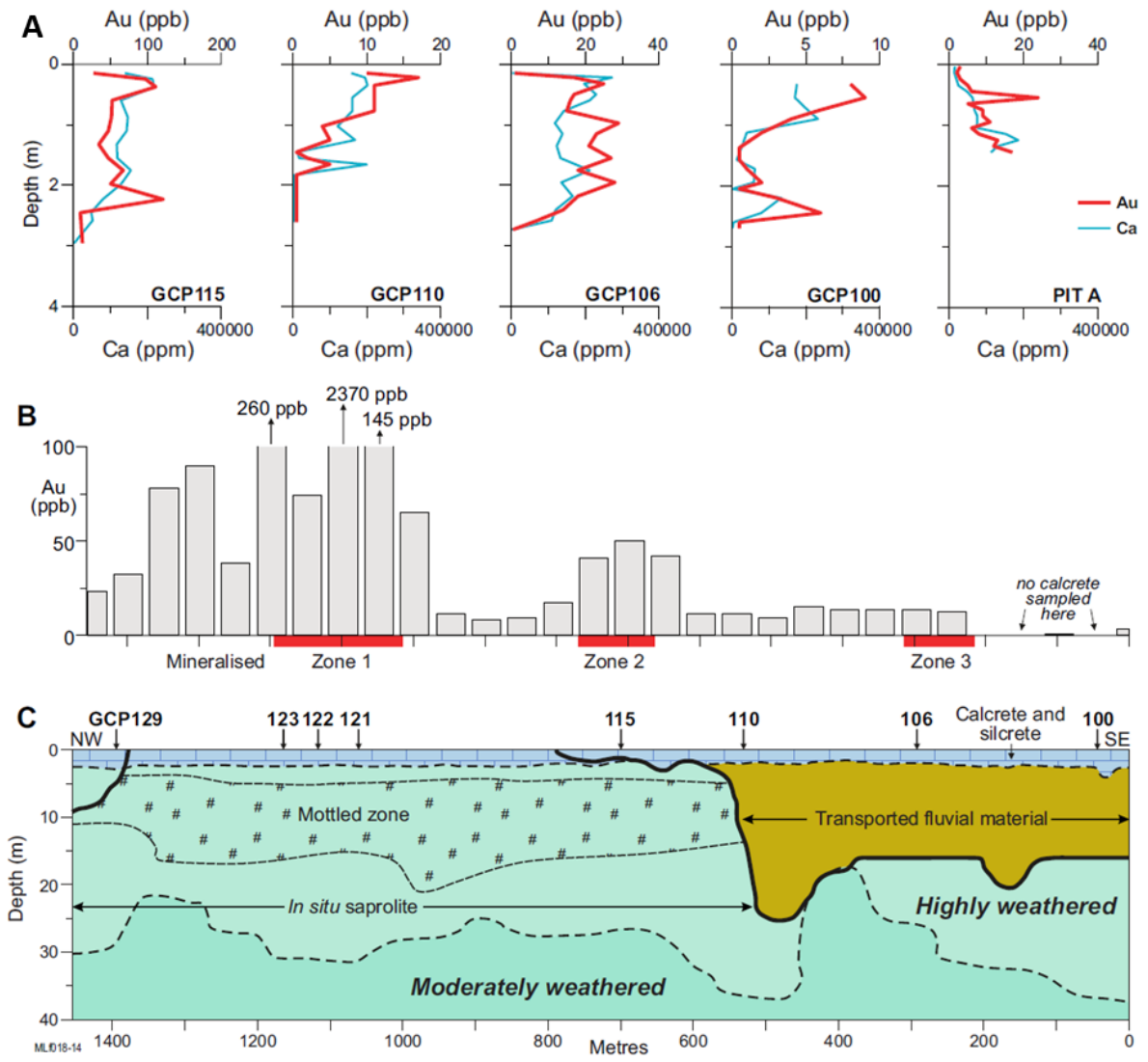


Figure 25. A: vertical profiles of Au and Ca in calcrete samples within the Challenger deposit. B: Au data from calcrete and C: regolith stratigraphy and location of soil pit. (Modified from Lintern, 2015).

5.2 General geology and the potential for Kraaipan gold exploration

Close to the international border with South Africa, it is evident that the BIF occurs as two parallel linear strips, of which the eastern one seems to disappear along strike towards the north (Figure 7 and 21). Given that all three formations of the Kraaipan Group contain BIF, it is unclear which, if any of the apparent BIFs belong to the Goldridge Formation, within which gold mineralisation at the Kalgold mine is known to be hosted. At most, only two BIF units are discernible from the magnetic data. Therefore, it is possible that not all of the BIFs of the three Kraaipan Group formations are present. If they are all present, the BIF units are indistinguishable even in areas where high-resolution magnetic data is present. In either case,

targeting of a specific BIF unit from magnetic data seems to be challenging if not impossible, complicating exploration targeting.

It is also evident from the magnetic data that there are discontinuities and displacement of the BIFs (and possibly the associated greenstone rocks) along strike, by faults with a lateral component (Figure 7 and 21). It is possible that erosion may have accompanied the discontinuous nature of the BIFs, thereby not only reduced the original BIF volume but also reduced or entirely eliminated any supergene gold enrichment that may have existed. (Supergene gold mineralisation was the focus of mining activities at Madibe mine, which closed in the 1930's).

Twenty of the boreholes used for interpolation of the Kalahari isopach map were located in the north-western part of the study area where high-resolution magnetic data was collected (Figure 8). All of these boreholes were drilled through the Kalahari cover and 20-30 m into the underlying bedrock. Logged sub-Kalahari lithological information has been integrated with the magnetic intensity map (Figure 26a) to come up with the geological map of the area, as depicted in Figure 26b. This was done by studying the magnetic signatures of the intersected bedrock and extrapolating the geology throughout the area of interest. Figure 26c shows an FVD magnetic image on which possible granitic plutons have been outlined as per the interpretation of the magnetic data.

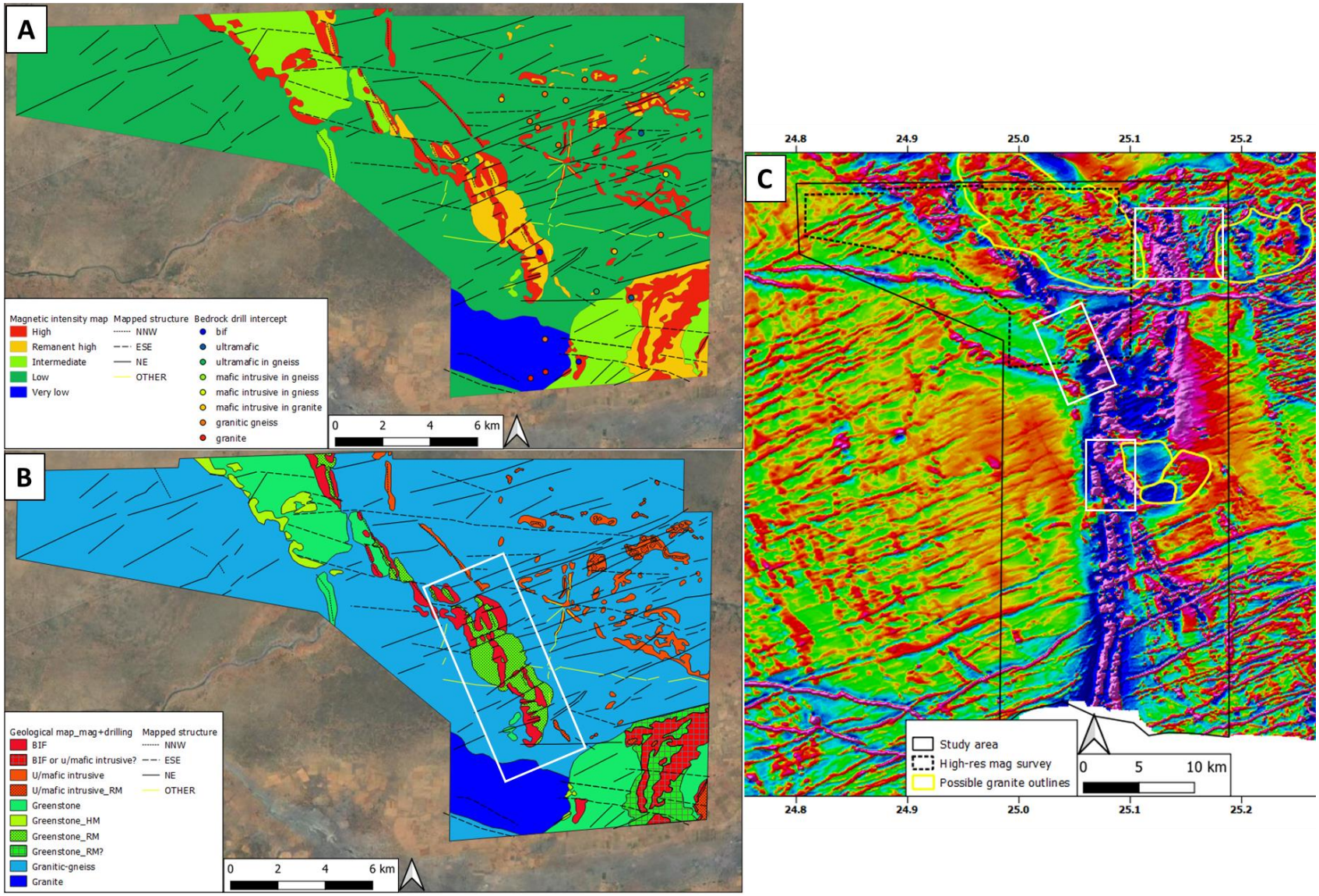

A
Magnetic intensity map
High
Remanent high
Intermediate
Low
Very low
Mapped structure
NNW
ESE
NE
OTHER
Bedrock drill intercept
bif
ultramafic
ultramafic in gneiss
mafic intrusive in gneiss
mafic intrusive in gniess
mafic intrusive in granite
granitic gneiss
granite
0 2 4 6 km
B
Geological map_mag+drilling
BIF
BIF or u/mafic intrusive?
U/mafic intrusive
U/mafic intrusive_RM
Greenstone
Greenstone_HM
Greenstone_RM
Greenstone_RM?
Granitic-gneiss
Granite
Mapped structure
NNW
ESE
NE
OTHER
0 2 4 6 km
C
24.8
24.9
25.0
25.1
25.2
Study area
High-res mag survey
Possible granite outlines
0 5 10 km

Figure 26. Interpretation maps of the NW area of the Kraaipan Greenstone Belt in Botswana where high-resolution magnetic data was collected. (a): magnetic intensity map overlain with borehole locations whose bedrock intercepts are shown in the legend. (b): geological map created from magnetic data and drilling data. (c): FVD magnetic image with outlines of possible granitic plutons shown in yellow. The white rectangles in all the maps outline areas of potential interest for gold exploration. U/mafic = mafic-ultramafic, RM = reversely magnetised, HM = highly magnetic.

According to Groves et al. (2018), world-class orogenic gold deposits are generally hosted in secondary structures, adjacent to primary faults and shear zones. Within the study area, such primary structures (which are the highly magnetic linear features in Figure 26c and NW faults in Figure 26b) are considered to be faults that are parallel to the strike direction of the greenstone. These structures formed during the accretion of Kimberly and Witwatersrand Blocks along the now Carlsberg Lineament (Adomako-Ansah et al., 2013). They pre-date those structures which are evident throughout the strike of the competent and chemically favourable BIFs.

Areas of potential interest for gold exploration have been outlined by white polygons in Figure 26. Firstly, the areas are proximal to the possible granitoids in Figure 26c. Groves et al. (2018) noted that the complexities related to granitic intrusions, such as contact points between greenstone and granite, or granite-granite contacts are potential sites of gold mineralisation, particularly in an Archaean setting. The granite-greenstone contacts depositional sites are related to resultant stress heterogeneities, while-granite-granite contacts offer favourable triple or quadruple-point junctions. The ductile greenstones are usually thickened at these contact points. Such Y and V-shaped zones represent strain gradients between the compressional zone of thinning within the high-strain. They have been observed in deposits such as Mussel White and Barberton Goldfields (Groves et al., 2018). Secondly, triple point junctions can be caused by inflection points of the greenstones themselves. In the study area, the vicinity where the KGB develops a NW extension (Figure 26c) is a potential target area. A structural disruption is likely to have taken place at the inflection and therefore BIFs occurring in that region are worth exploring for gold mineralisation. Thirdly, a zone of sigmoidal shaped greenstone-BIF occurrence is outlined in Figure 26b. It resembles boudinaged and dismembered pod-like features such as those which contain gold mineralisation at Blue Dot (Anhaeusser, 1991). Such zones of gold deposition are usually formed during failure of rotating competent lithologies and reactivation of pre-existing structures leading to dilation (Groves et al., 2018).

Higher drilling density would have resulted in a more accurate interpolation of the Kalahari isopach map. However, the current version of the Kalahari isopach map can be used to define areas of thinner and thicker cover, with areas of thinner cover being more advantageous for mineral exploration and future exploitation. Therefore, the map can be used to target areas for focussed exploration. There is an indication that Kalahari cover thickness within the study area is related to basement architecture to some extent. Some isopachs sub-parallel sections of the basement faults, which may have had more control on the bedrock topography than the response of bedrock lithology to weathering and erosion. If true, it would follow that fault mapping can be essential not only for understanding the structural geology of a given area but also overburden thickness, where it is present and crucial to constrain.

High-resolution satellite imagery was useful in identifying the outcrop extent of the BIF and allowing for it to be outlined in detail. Folds and faults were also mapped from this data, which allowed for focussed field mapping over the most interesting areas. Landsat 8 remote sensing data was useful in identifying reflectance signatures associated with certain types of regolith, which aided the understanding of the spatial distribution of the regolith within the study area. In some places, the regolith types appear to have been misclassified (e.g., distribution of speckles of BIF within the ploughing fields, Figure 14), but this was useful in indicating the most probable provenance of the regolith. If geochemical anomalies are present in those regolith types, not only would they be known to have been transported, but there could be clues as to their provenances. Although the Landsat 8 data was helpful in basic mapping of rock exposures, it could not map geology under cover.

Only nickel and copper were analysed along with gold during the “Soil Sampling 1” programme. These are not atypical pathfinder elements for gold in orogenic settings therefore their unclear association with gold was not surprising. This programme was conducted close to outcropping BIFs. The Soil sampling 2 programme was conducted over areas of relatively thicker soil cover, which may in part explain the low metal contents recovered from the samples.

Metal recoveries were also interpreted over magnetic imagery. No obvious associations were made between different metals and underlying magnetic signatures. Therefore, no obvious litho-geochemical trends were observed. The apparent absence of these trends is possibly

related to poor metal recoveries. There were however metal trends associated with topographical features. For instance, the highest concentrations of Ag, Au and Ni are located proximal to drainages (Figure 20). These potentially anomalous occurrences are likely to have been transported from elsewhere. Stream sediment sampling is therefore only likely to produce ambiguous geochemical soil results with no discernible source and is therefore not recommended. Poorly developed drainage in the area also suggests against this sampling method.

Just like in the Gawler Craton, calcrete regolith is abundant in the Kraaipan granite-greenstone terrane. Efforts should be made to understand it better and use it routinely as a sampling medium for gold exploration as has been done in Australia since the discovery of the Challenger deposit Challenger deposit (Williams et al., 2003 and Lintern, 2015). Okujeni et al. (2005) conducted calcrete sampling at Kalgold and Blue Dot. As depicted in Figure 27, there seemed to be a positive association between calcrete and gold, with gold anomalism occurring in laminated calcrete. Although the anomaly is not as pronounced as that of the Challenger deposit (at a maximum of 2370 ppb), it exists nonetheless.

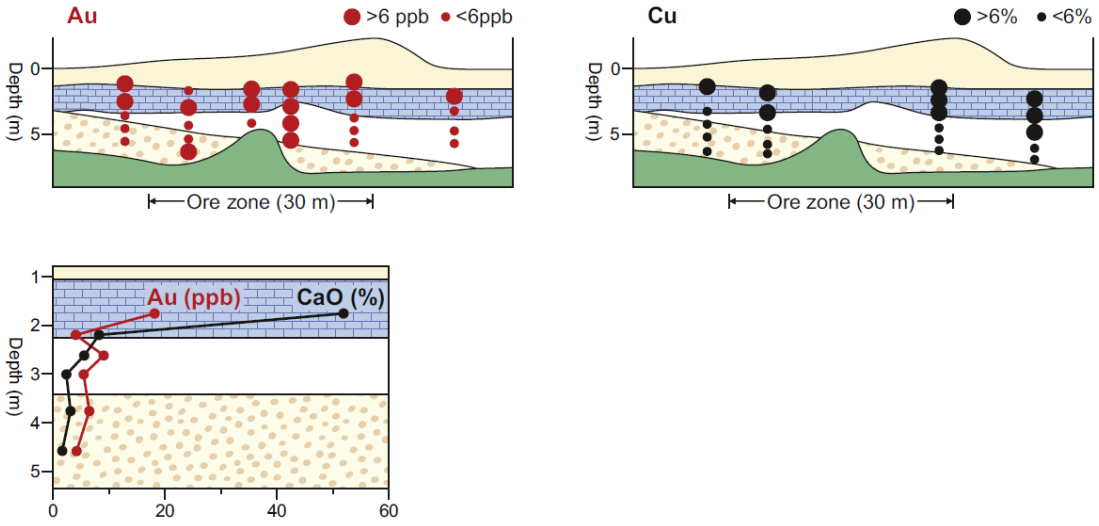


Figure 27. Distribution patterns of selected elements in regolith along a section overlying the D-Zone orebody of Kalgold mine. Top to bottom geology of regolith in all sections: aeolian sand, laminated calcrete, calcified sand, calcified pebbly sand and mineralised BIF/greenstone. From Lintern, (2015).

No known geochemical calcrete sampling programmes have been carried out in the Kraaipan Terrane setting since this study. It should however, be carried out routinely in order to explore its full potential in the area. Outside of Australia, calcrete sampling has proven worthwhile in

the recent years in Namibia for gold exploration in Damaran stratigraphy (Osino Resources, 2021). Some of the possible challenges of calcrete sampling technique in the Kraaipan Terrane could be: thick unconsolidated overburden which would increase the expense of recovering underlying calcrete samples; thick calcrete horizons which would require elaborate drilling techniques; complex/heterogeneous calcrete horizons which may complicate or make impossible the interpretation of geochemical results.

Geochemical data from drill intersections suggest that gold is only elevated within rocks that have greater than 15% iron. These intersections may be associated with rocks that have strong iron alteration or more likely, BIF. Silver, copper, nickel, arsenic, antimony, selenium and bismuth are closely associated with gold. These metals are therefore likely to be good pathfinders for gold in the KGB and should form part of multi-element analysis packages for future sampling and/or drilling. Depending on how reworked the regolith is, and the mobility of these elements within it, they may or may not be effective pathfinder elements in it. Research to that effect is nonetheless lacking in the Kraaipan Terrane.

6 Conclusions

Magnetic data proved excellent in differentiating the greenstone rocks, particularly BIF, from surrounding granitoids. It has allowed for identification of potential target areas for gold mineralisation which include: (I) granite-greenstone rock as well as granite-granite contacts, which are zones of strain gradients created by competency contrast and geometries of granitic intrusions (and particularly proven in Archaean systems to host gold mineralisation); (II) a point of inflection of the KBG into a NW extension of the belt (the belt extension has been suspected previously, and now confirmed conclusively). Structural disruption is likely to have occurred at that inflection point and may have resulted in development of a structure that is oblique to, and intersects belt-parallel primary structures and (III) a sigmoidal-shaped zone of probable boudinaging of the BIF and greenstone rocks within the NW extension of the KGB. Dilatational zones such as this one host gold mineralisation at Blue Dot mine and elsewhere. Association with BIF improves the interest of that area due to the chemical and rheological favourability of this rock unit for gold mineralisation.

Assessment of limited multi-element data from the boreholes that contained elevated intersections of gold suggests a close downhole correlation of gold with iron, silver, copper, nickel, arsenic, antimony, selenium and bismuth. More downhole multi-element data is needed to assess if this is truly the case. If so, these elemental associations with gold also need to be investigated within the regolith as this is the most practical sample medium for mineral exploration.

The created Kalahari isopach map shows that regolith is thick in some parts of the study area, and in those places, surface sampling is unlikely to be effective. The map is still coarse in some places and work is required to improve it by: sourcing geological information for the available boreholes that lack it; incorporating additional drilling data and; applying other complementary methods such as Euler models. Kalahari isopach maps should be routinely applied in target selection and area prioritisation.

Calcrete sampling has proven invaluable in Australia for gold exploration, and it must not be overlooked in the study area, where calcrete is sufficiently abundant. Understanding of exploration results from this type of geochemical sampling requires a good understanding of the present regolith, but this is lacking and is required for the study area. High-resolution

orthophotos and remote sensed images could in part be helpful with this task as they were certainly useful with geological mapping.

7 References

Adomako-Ansah, K., Mizuta, T., Hammond, N.Q., Ishiyama, D., Ogata, T. and Chiba, H. 2013. Gold mineralization in banded iron formation in the Amalia Greenstone belt, South Africa: A mineralogical and sulfur isotope study. Resource Geology, 63, 119–140.

Anhaeusser, C., R. 1991. The Archean Kraaipan Group volcano-sedimentary rocks and associated granites and gneisses of the South-Western Transvaal, Northwestern Cape Province and Bophuthatswana - Excursion guidebook. University of the Witwatersrand, South Africa.

Anhaeusser, C., R. and Walraven, F. 1997. Polyphase crustal evolution of the Archean Kraaipan greenstone-granite terrane, Kaapvaal Craton, South Africa. Economic Geology Research Unit Information Circular No. 313.

Brandl, G., Cloete, M. and Anhaeusser, C.R. 2006. Archaean greenstone belts, In: M.R. Johnson, C.R.Anhaeusser and R.J. Thomas (Editors), The Geology of South Africa. Geological Society of South Africa, Johannesburg/Council for Geosciences, Pretoria, 9–56.

Caddey, S., W., Bachman, R., L., Campbell, T., J., Reid, R., R. and Otto, R., P. 1991. The Homestake Gold Mine, an early Proterozoic Iron-Formation-hosted fold deposit, Lawrence County, South Dakota. U.S. Geological Survey Bulletin, 1857-J.

Carney, J., N., Aldiss, D., T., and Lock, N., P. 1994. The geology of Botswana. Bulletin of the Geological Survey of Botswana, 37.

Dart, R., C. 2009. Gold-in-calcrete: A continental to profile scale study of regolith carbonates and their associate gold mineralisation. PhD Thesis, Geology and Geophysics School of Earth and Environmental Sciences, The University of Adelaide, (unpublished).

Elburg, M.A. and Poujol, M. 2020. Lu-Hf analyses of zircon from the Makoppa Dome and Amalia-Kraaipan area: implications for evolution of the Kimberley and Pietersburg blocks of the Kaapvaal Craton. South African Journal of Geology, 123.3, 369–380.

Groves, D., I., Santosh, M., Goldfarb, R., J. and Zhang, L. 2018. Structural geometry of orogenic gold deposits: Implications for exploration of world-class and giant deposits. Geoscience Frontiers, 9, 1166–1177.

Haddon I., G., 2005. The sub-Kalahari geology and tectonic evolution of the Kalahari basin, Southern Africa. PhD Thesis, Faculty of Science, University of the Witwatersrand (unpublished).

Hammond N., Q., 2002. The geochemistry of ore fluids and controls of gold mineralization in Banded Iron Formation at the Kalahari Goldridge Deposit, Kraaipan Greenstone Belt, South Africa. PhD Thesis, Geology Department, Rhodes University (unpublished)

Hammond, N.Q. and Moore, J.M. 2006. Archaean lode gold mineralisation in banded iron formation at the Kalahari Goldridge deposit, Kraaipan Greenstone Belt, South Africa. Mineralium Deposita, 41, 483–503.

Hammond, N.Q. and Morishita, Y. 2009. Source of ore fluids at the Kalahari Goldridge deposit, Kraaipan greenstone belt, South Africa: evidence from Sr, C and O isotope signatures in carbonates. Geofluids, 9, 356–364.

Keyser, N. and Du Plessis, C., P. 1993. The geology of the Vryburg area. Explanation Sheet 2624 (1:250 00) Vryburg. Geological Survey of South Africa.

Lintern, M.J. 2015. The association of gold with calcrete. Ore Geology Reviews, 66, 132–199.

Mapeo, R.B.M. 2004. SHRIMP U-Pb zircon ages of granitoids from the Western Domain of the Kaapvaal Craton, Southeastern Botswana: implications for crustal evolution. South African Journal of Geology, 107, 159–172.

Mapukule, L., E. 2009. Interpretation of the regional geochemical data as an aid to exploration target generation in the North West Province, South Africa. MSc Thesis, Department of Geology, University of Fort Hare (unpublished).

Morelli, R.M., Bell, C.C., Creaser, R.A. and Simonetti, A. 2010. Constraints on the genesis of gold mineralization at the Homestake Gold Deposit, Black Hills, South Dakota from rhenium osmium sulfide geochronology. Mineralium Deposita, 45, 461.

Okujeni, C.D., Ackon, P., Baugaard, W. and Langa, N. 2005. Controls of element dispersion in aeolian sand and calcrete-dominated regolith associated with gold mineralization in the Kraaipan greenstone belt, South Africa. Geochemistry: Exploration, Environment, Analysis, 5, 223–231.

Osino Resources, 2021. Twin Hills Gold Project, Namibia. NI 43-101 Technical Report.

Pearton, T. and Viljoen, M., 2017. Gold on the Kaapvaal Craton, outside the Witwatersrand, South Africa. South African Journal of Geology, 12.1 101-132.

Poujol, M. 2005. New U-Pb data on zircons from the Amalia greenstone belt Southern Africa: insights into the Neoarchaean evolution of the Kaapvaal Craton. South African Journal of Geology, 108, 317–332.

Poujol, M., Hirner, A.J., Armstrong, R.A. and Anhaeusser, C.R. 2008. U-Pb SHRIMP data for the Madibe greenstone belt: implications for crustal growth on the western margin of the Kaapvaal Craton, South Africa. South African Journal of Geology, 111, 67–78.

Ramotoroko, C.D., Ranganai, R.T. and Nyabeze, P. 2016. Extension of the Archaean Madibe-Kraaipan granite-greenstone terrane in southeast Botswana: Constraints from gravity and magnetic data. Journal of African Earth Sciences, 123, 39–56.

Ranganai, R.T., Moidaki, M.D., King, J.G. and Bagai, Z.B. 2017. Geophysical and hydrogeological groundwater prospectivity mapping in the Kraaipan granite-greenstone terrain, southeast Botswana. Journal of Water Resource Protection, 09, 1270–1298.

Reunion Mining Botswana (Pty) Ltd. 1998. Prospecting License 57/96. Geological Survey of Botswana, Lobatse.

Steadman, J., A. and Large, R., R. 2016. Synsedimentary, Diagenetic, and Metamorphic Pyrite, Pyrrhotite, and Marcasite at the Homestake BIF-Hosted Gold Deposit, South Dakota, USA: Insights on Au-As Ore Genesis from Textural and LA-ICP-MS Trace Element Studies. Economic Geology, 7, 1731–1752.

Steadman, J., A., Large, R., R., Davidson, F., J., Bull, S., W., Thompson, J., Ireland., T., R. and Holden, P. 2014. Paragenesis and composition of ore minerals in the Randalls BIF-hosted gold deposits, Yilgarn Craton, Western Australia: Implications for the timing of deposit formation and constraints on gold sources. Precambrian Research, 234, 110–132.

Williams, P., Frances, D., Gillman, J. and Bonwick, J. 2003. Geophysical characterisation of the Challenger gold deposit, Gawler Craton, South Australia. ASEG Extended Abstracts, 3, 19-27,